UNIVERSITÀ POLITECNICA DELLE MARCHE

Department of Engineering

Master Degree in Biomedical Engineering

Thesis:

Indirect quantitative assessment of the respiratory frequency from heart rate during physical exercise

Valutazione quantitativa indiretta della frequenza respiratoria da quella cardiaca durante l'esercizio fisico

ADVISOR:

Prof. Laura Burattini

CO-ADVISOR:

Prof. Micaela Morettini

Prof. Massimo Sacchetti (University of Rome Foro Italico)

CANDIDATE:

Benedetta Pambianco

A.Y. 2019-2020

Abstract:

Respiratory rate (RF) and its variation is one of the marker for monitoring the state of health of a subject. Furthermore, it has been demonstrated that RF can also be considered a marker of the physical effort during exercise. In some situations, a reliable measurement of the RFs is required and these values may be measured through wearable sensors, which are becoming desirable for healthcare applications, such as the management of chronic diseases. However, not all wearable sensors are able to estimate directly and continuously the RF. Therefore, the idea is to extract indirectly the respiratory signal, from which to estimate subsequently the RF, from the electrocardiogram (ECG), generating the ECG-Derived Respiration (EDR) signal. The aim of the present study is to present a new method based on the Segmented-Beat Modulation Beat (SBMM), which through a mathematical modelling procedure, is able to provide an indirect quantitative assessment of the RF from the heart rate (HR) during physical exercise. Clinical data was collected and provided by University of Rome Foro Italico. Data consists of RFs measured through a metabolimeter, which constitute the gold standard, and ECG signals from nine healthy subjects. Subjects were involved in a graded exercise test on a cycle ergometer, in which exercise intensity was progressively increased. The large range of HRs and the RFs collected during the protocol were interpolated by a double exponential curve and used to define a model, whose purpose is to increase the accuracy of the RF estimate from the EDR. To test its reliability, the model was tested in the EDR extraction on the same subjects used for its definition. Two parallel processes were performed in the study: EDR extraction and the RF frequency band definition. Starting from EDR extraction, for each subject, the ECG modulated by the respiration was the input to the modified SBMM (mSBMM), specifically designed for the EDR extraction. The original SBMM allows to obtain a clean ECG from a noise corrupted ECG tracing. The EDR was obtained by subtraction between the original ECG modulated by respiration and the clean ECG, provided as output from mSBMM. The Fourier spectrum of the EDR was obtained. In the second process, the subject HR was the input to the model, allowing the definition of a theoretical RF. From this value, the frequency band centred on the expected RF and with a width of 10 cpm was defined. As final step, the RF was identified as the frequency at which the EDR spectrum had maximum in the previously defined RF frequency band. Results showed that the median RF values of EDR and reference RF distributions were 26.2 cpm and 24.4 cpm, respectively. Among all subjects, the median value of the correlation coefficient was 0.8, underling a strong agreement between the two distributions. Median absolute error was equal to 1.4 cpm, which an acceptable error during physical exercise. In the majority of the cases, the median relative error calculated with respect the reference RF were lower than 10%. Wilcoxon signed-rank test confirmed that on average the two distribution were not statically different. Thus, the proposed procedure, which involves the combined use of both mSBMM and the model, allows a reliable EDR estimation and RF identification during physical exercise.

Index:

Introduction

Respiratory rate (RF) and its variability have proved to be good indicators of the health condition changing in the patients and play a crucial role in identifying the onset of health problems, in combination with other vital parameters [1]. In fact, RF has numerous clinical uses, being one of the most important vital parameters and it is the main cause of HR modulation [2]. For example, tachypnea (a significant increase of the respiratory rate compared to the norm) is one of the most important factors for predicting cardiac arrest.

Despite their importance, RF has received little consideration not only in clinical settings, but also during training. In fact, the RF has a significant role during physical activity as a powerful marker of physical effort, even more than other usually measured physiological parameters [3]. RF time course is closely associated with that of Rating of Perceived Exertion, a quantitative measure of the perceived exertion during physical activity. Changes in RF may highlight important implications for training and recovery monitoring [3]. For these reasons, the RF monitoring, together with all the other variables, is starting to be encouraged by sport scientists and physicians [3].

Seen its role as marker of both state of health and physical effort, there are situations in which respiratory signal and the RF should be monitored in a continuously and reliable way, such as in the hospital intensive care unit. Similarly, the same need can occur, although in a less stringent way, in healthcare applications, such as telemedicine and the management of chronic diseases. In these last contexts, the use of wearable devices is becoming of great relevance in order to minimize the invasiveness and maximize comfort. However, only a small number of wearable sensors are capable of continuously measuring RF and comparing it with other key physiological parameters such as HR, temperature and oxygen saturation level in the blood [4].

The extraction of the respiratory signal through indirect methods, such as through the acquisition of the electrocardiogram (ECG), allows the recording of a single signal, from which it is possible to obtain all the data of interest.

The indirect extraction of the respiratory signal from the ECG implies the analysis of interaction between two different systems: the cardiovascular and the respiratory systems. Cardiac activity and respiration can be considered as part of a complex non-linear dynamical system based on two weakly coupled oscillators (heart beating and breathing movement) coupled by several structural and functional types of cardiorespiratory interaction. These interactions involve a complex interplay between the brainstem activity (where the automatic nervous system and the respiratory drive are the main elements), the heart and lungs in the thoracic cavity, and the vascular system [5].

The search for patterns in the human heartbeat sequence is a highly studied topic. Breathing, which is more under direct conscious control than heartbeat, is much less studied. The problem with searching for a breathing-heartbeat correlation is that these systems have very different rhythms. The heart normally beats 60 to 70 times per minute, while the breathing rate is about one-fifth of that. Furthermore, the heart and breathing phenomena are complex; consequently at least for periods of awakeness or rapid-eye-movement (REM) sleep little or no phase synchrony (that is, breathing and heartbeat recurring with a consistent relation to each other) can be found [6].

In literature, many algorithms are present for the ECG-derived respiratory (EDR) signal extraction. The conventional methods, which provide for the calculation of the area of the QRS complex and the arctangent of the relationship between them, assuming that the I and III lead form a right angle, are still used. However, the I and III leads are not exactly orthogonal (the augmented lead VF forms a right angle with the I lead) and the result of the arctangent is not always the optimal EDR since the location of the heart is different from individual to individual. The fact that they are not orthogonal involves the presence of a systematic error in estimating the direction of the average cardiac electrical axis [7]. It has also been hypothesized that in the presence of noise and cardiac dysfunctions, the morphology of the QRS complex is not reliable for providing information on breathing; it is necessary to select a shorter interval around the R peak. If true, this would penalize the methods that consider the entire QRS interval and extract a series of angles by joining the information of both leads [8]. In recent research, it has been established that single-lead estimates are more robust than methods based on the average cardiac electrical axis. In fact, the effects of breathing on ECG modulation depend on the respiratory characteristics of the subjects (if in presence of a thoracic breathing or an abdominal breathing for example), on the position of the heart and relevance of the rotation [8].

Moreover, in some cases, the RF estimation from EDR may be challenging, especially during physical exercise or wearing wearable sensors. In fact, motion artefacts and superimposed noises may compromise the respiratory signal and the subsequent RF calculation.

Therefore, the aim is to propose a new procedure based on the Segmented-Beat Modulation Method [9], which through a mathematical modelling procedure, is able to provide an indirect quantitative assessment of the RF from the HR during physical exercise. In fact, in the present study the definition of a model is introduced, in which the RF is expressed as function of HR. Since the relationship between the HR and RF is affected by several factors, the purpose of this model is the individuation of a plausible range of RFs starting from the subject HR obtainable from ECG. The identification of a range in which individuate the RF could be an important topic, especially during physical activity or wearing wearable sensors. The range individuated by the proposed model was then used in order to increase the accuracy in RF assessment in situations other than that at rest, which is the final goal of the study.

Chapter 1: Cardio-Respiratory Systems and their Biosignals

1.1 Cardiovascular System

The cardiovascular system is made up of a central organ, the heart, and different blood vessels, which are the arteries, veins and capillaries. The heart, a muscular organ, pushes the blood into the arteries; these distribute it to all the organs of the body and then they branch out into capillaries. The capillaries, vessels with very thin walls, allow metabolic exchanges and therefore give rise to the veins, by means of which the blood returns to the heart. The heart is a hollow organ divided into two halves (right and left) not communicating with each other. Each half is made up of two superimposed and communicating cavities: the upper atrium and the lower ventricle. The right half contains venous blood, rich in carbon dioxide; the left half arterial blood, rich in oxygen [10].

The circulatory system is divided into two main sectors called systemic circulation and pulmonary circulation. The systemic circulation begins from the left ventricle of the heart with the aorta artery, a large vessel that with its numerous branches distributes arterial blood within the body. The branches of the artery within the organs branch out into the blood capillaries at which, through exchanges with interstitial fluids, the arterial blood releases oxygen and picks up carbon dioxide, turning into venous blood. From the capillaries the veins are formed which, converging gradually, reach the superior vena cava, the inferior vena cava and the coronary sinus, which reach the right atrium of the heart where the systemic circulation ends. The venous blood from the right atrium then passes into the right ventricle entering in the pulmonary circulation. The pulmonary circulation, begins from the right ventricle of the heart with the pulmonary artery which, bifurcating, carries venous blood, rich in CO_2 to the lungs. The pulmonary artery branches out into capillaries, in which the venous blood loses CO_2 acquires O_2 and becomes arterial blood. Arterial blood returns to the heart with the four pulmonary veins that reach the left atrium, where the pulmonary circulation ends. From the left atrium, the arterial blood then passes into the left ventricle to resume the path of systemic circulation. The pulmonary circulation is therefore characterized by venous blood in the arteries and arterial blood in the veins [10].

The function of the blood circulatory system is to ensure a continuous supply of oxygen and nutritional materials to all organs by simultaneously taking catabolites from them, i.e. carbon dioxide, ammonia, urea, uric acid and other substances [10].

1.1.1 Anatomy of the heart

Internally the heart is divided into four cavities, functionally paired two by two (Figure 1). Each pair of cavities consists of an atrium, with a thin wall and located above, and a ventricle, with a thicker wall and placed below, connected through an atrio-ventricular orifice equipped with a heart valve. The two pairs of cavities are separated by a cardiac septum. Each atrium communicates with the corresponding ventricle through the atrioventricular orifice which is equipped with a cuspidate valve [10].

The fibrous skeleton of the heart allows the anchor of the muscle bundles that make up the wall of the atria and ventricles [10].

The orifices that connect the ventricular cavities with the efferent vessels are also protected by valves that prevent reflux: pulmonary semilunar valve in the right ventricle for the pulmonary artery, aortic semilunar valve in the left ventricle for the aorta. The tricuspid valve is the right atrioventricular valve and practically forms the floor of the atrium; it fits on the fibrous ring of the right atrioventricular ostium and is composed of three flaps, hence the name. In the upper wall of the left ventricle, there is the bicuspid valve, with the anterior and posterior cusps (flaps), and the aortic valve, with the three aortic semilunar valves, which gives access to the ascending aorta [10].

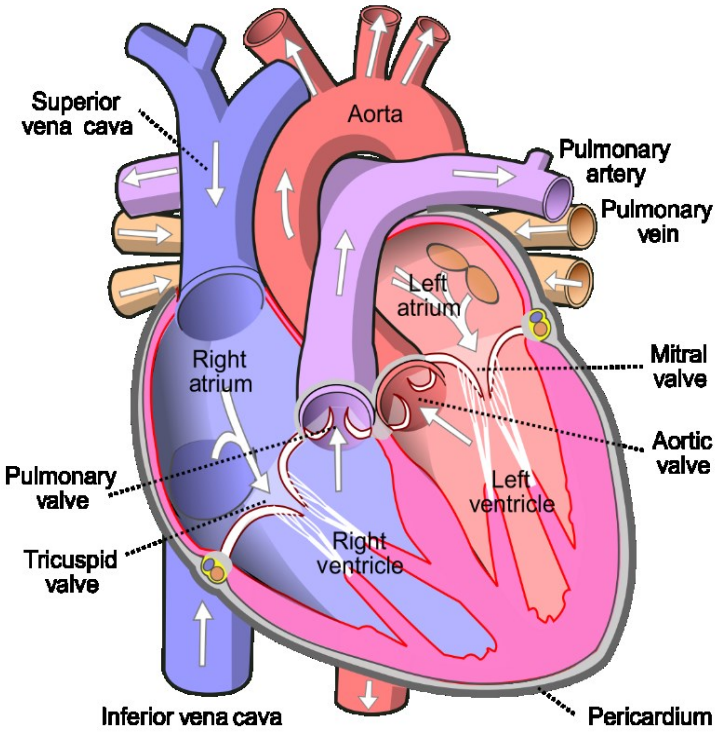

Figure 1. The heart

1.1.2 Physiology of the heart

As known, the heart is a double pump made up of the four chambers as described above. The two atria, the upper chambers, contract almost simultaneously; the ventricles, the two lower chambers, have the same behavior. The right atrium receives venous blood from the superior and inferior caval veins and pumps it to the right ventricle. This in turn pushes the blood into the lungs, where it is oxygenated. Upon returning from the lungs, blood enters the left atrium from where it is pushed into the left ventricle. This contracting pushes the heart into the aorta from where it is distributed through the arteries to the body. Finally, through the capillaries, it is brought back to the two hollow veins which reach the right atrium [10].

The rhythmic action of the heart is controlled by an electrical signal that originates in some specialized cells. These constitute the conduction system of the heart. The conduction system of the heart consists of a particular specific myocardial tissue, which functionally connects the muscles of the atria with the muscles of the ventricles (Figure 2). This specific myocardium is made up of myocardial cells that have lost their contractile properties by specifically acquiring conductivity functions. The specific myocardium represents the site in which the contraction stimuli of the heart arise and it is the way through which the stimuli themselves spread to the common myocardium. The conduction system consists of two sectors: the sinoatrial sector and the atrioventricular system [10].

The first begins with the sinoatrial node in the upper wall. It is called a pacemaker because it automatically stimulates the heart to contract. These stimuli propagate along bundles of specific myocardial cells that extend from the sinoatrial node into the common myocardium of the atrial walls. In this way the atria can contract simultaneously (*atrial systole*) and the contraction wave propagates so as to push the blood into the underlying ventricles. The inter-nodal bundles also depart from the sinoatrial node and carry the stimuli that induce contraction in the atrioventricular system [10].

The atrioventricular conduction system begins with the *atrioventricular node*. A bundle of specific cells departs from the node, the bundle of His, which through the right fibrous trine reaches the interventricular septum and reaches the muscular wall of the septum and divides into two branches, right and left. The branches of the atrioventricular system also result in a series of small bundles, which intertwining with each other, go up towards the walls of the ventricles, forming the Purkinje fibers, one per ventricle. By means of the Purkinje fibers, stimuli propagate to the common ventricular myocardium which contracts by pushing the blood into the pulmonary and aortic arterial orifices [10].

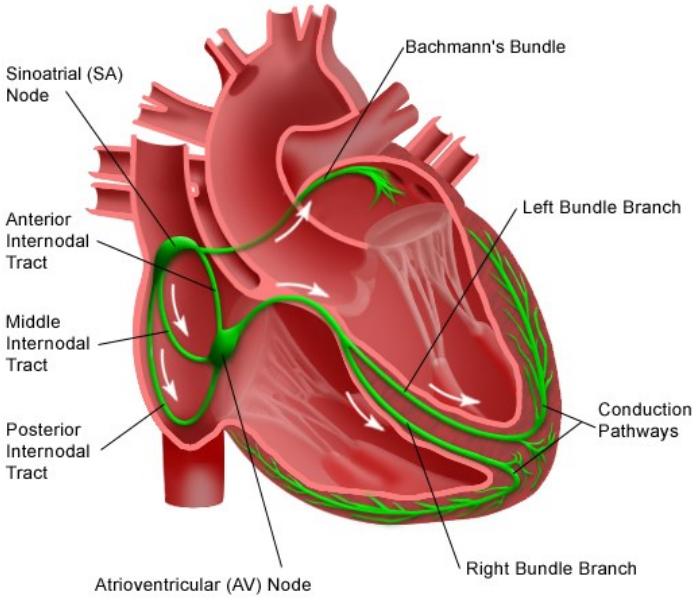

Figure 2. Electrical System of the Heart

1.1.3 Electrocardiogram

The nerves and muscles that make up the heart can be considered as a source of electric charges which travel within a conductor that is the chest. The electric field produced by these moving charges - which actually are in the process of depolarization and repolarization of the heart muscle - emerges on the surface of the chest with its equipotential lines. Therefore, if electrodes are placed on two lines of the field with different potential, on the thoracic surface (but in reality this field is detectable in the whole body), a difference in potential can be detected. This difference in potential varies just as the depolarization and repolarization of the heart fibers varies over time, and its recording as a function of time takes the name of an ECG. The relationship between the pumping action of the heart and the electrical potentials detectable on the body surface can be understood if it is considered that the heart muscle contracts, due to the effect of the propagation of the depolarization, along a certain position and that, as occurs along a nerve fiber that transmits an excitation, produces an ionic current (Figure 3), which in turn leads to a drop in potential between the two non-coincident places of the biological material in which it flows. In Figure 3, Rt indicates the generic electrical resistance of the external medium to the heart muscle (thorax). It shows the potential drop produced by the ionic current coming out and falling in the axons of the nerve network constituting the His bundle and the Purkinje network [11].

The distribution of potential that affects the entire heart muscle when the ventricles are half depolarized is shown in Figure 4. The letters A, B and C represent electrodes applied on the thorax and placed approximately at the vertices of an equilateral triangle. It is observed that the difference in potential detected depends on the position of the electrodes, and again, that the shape of the equipotential lines is that obtainable from a dipole consisting of two electric charges of opposite sign. This means that the electrical activity of the heart can be thought, in an abstract way, as

originating from a dipole, and therefore representable as a vector that varies cyclically over time in intensity and direction [11].

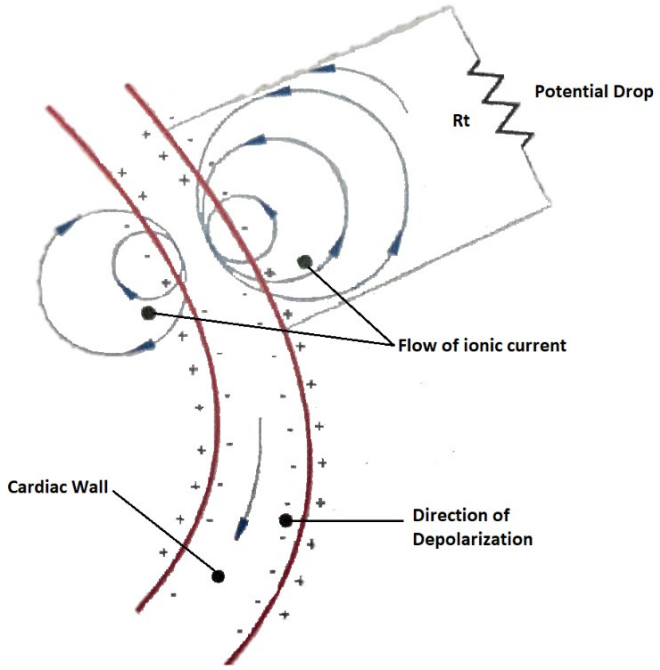

Figure 3. Effects of the propagation of depolarization [11]

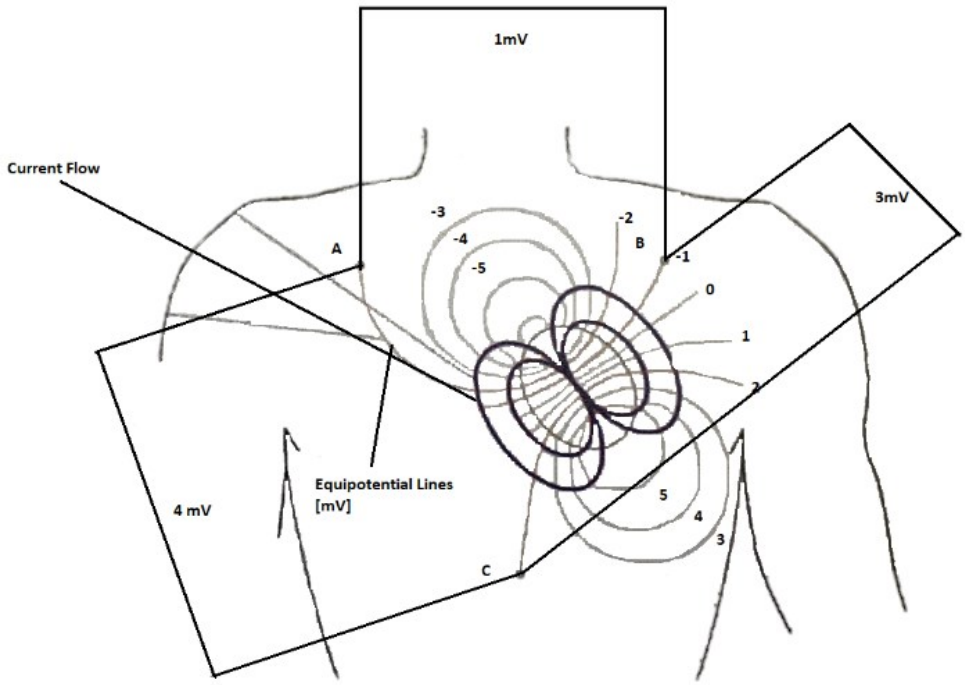

Figure 4. Chest potential distribution during the middle of the ventricle depolarization phase [11]

This is a fundamental concept and therefore it is convenient to expose in more detail:

- the origin of electrical potentials;
- their spatial distribution;
- the methods on the basis of which it is possible to detect and record such potentials in a repeatable and independent manner.

The propagation mechanism of the electrical impulse that starts from the atrioventricular (AV) node, once it has been excited by the sinoatrial node (SA), is such that the propagation speed in the two branches of the His bundle is different and in particular the left ventricle contracts with a modest delay (about 0.01 s) compared to the right ventricle. Depolarization proceeds on the internal surface of the wall of the ventricles towards the external surface, and from the apex of the heart towards the base of the ventricles. It follows that the map of the places where the negative and positive charges are found in a certain instant changes instant by instant. The fact that the entire system does not simultaneously depolarize and repolarize, means that the vector representative of the cardiac potential varies over time both in length (intensity or modulus) and in direction (angle or phase). To simplify the effect of the movement of the charges, it is convenient to attribute the presence of these electric fields as originating from the aforementioned dipole which takes the name of the *equivalent electric dipole of the heart* [11].

The electric potential E produced by a certain electric charge Q at a point P at a distance d from the electric charge itself, holds [11]:

$$E(d) = \frac{Q}{4\pi\xi\xi_r d^2} \tag{1}$$

with ξ_r dielectric constant of the medium and ξ dielectric constant of the vacuum ($8.859 \cdot 10^{-12}\, F \cdot m^{-1}$). It is possible at any moment to represent all the positive charges of the heart with a single positive charge (of a value equal to the sum of the existing ones) placed at a certain point inside the heart, and all the negative charges with a single negative charge, placed in another point. During the depolarization and repolarization process, the center of all the positive charges does not coincide with that of all the negative charges, and it is therefore possible to imagine the defined electric dipole (Figure 5) characterized by the following parameters [11]:

- quantity of electric charge;
- distance between the two charges;
- orientation of the line joining the two charges (dipole axis).

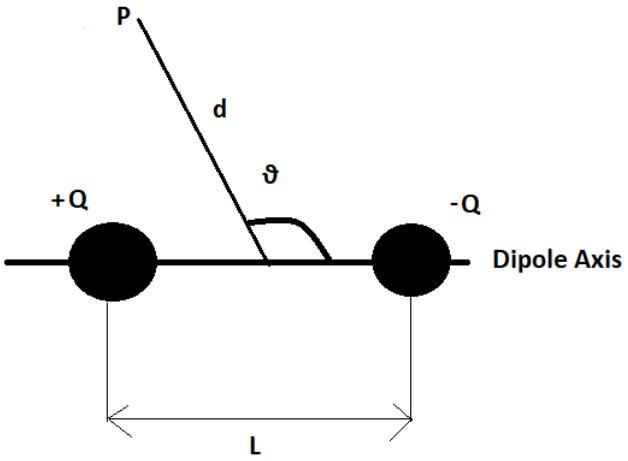

Figure 5. Cardiac Dipole [11]

From this, it follows that the electric potential E at a point in the space P located at a distance d much greater than the distance L between the two charges is provided by [11]:

$$E(P) = \frac{\mu cos\vartheta}{4\pi\xi\xi_r d^2} \quad (2)$$

where:

μ: dipole moment (con μ= Q·L);

Q: dipole charge;

d: distance of point P from the center of the dipole;

ϑ: angle between the dipole axis and the line joining the point P with the midpoint of L.

For what has been said, it is legitimate to study the evolution of the map of charges during the cardiac cycle in terms of change of the dipole which, due to its origin, is better referred to as an equivalent dipole, for which its electric moment μ and orientation of its axis vary from instant to instant. The equivalent dipole axis is called the *instantaneous electrical axis of the heart*. Since the dipole is characterized by an intensity (scalar quantity equal to the moment of the dipole μ) and by a direction (axis of the dipole), it can be represented by a *vector H* which is an expression of the sum (instantaneous) of the electrical activities of the heart [11].

The projections of H along certain directions are detectable in intensity and direction by means of potential difference measurements on the body surface. The detection and recording of cardiac potentials must be carried out by having at least two electrodes applied on the surface of the body and placed in non-equipotential places. Differences in recordable potentials depend on where the electrodes were placed. Therefore, it is essential that the positions where the electrodes are placed are standardized [11].

Einthoven first schematized the human body as a conductor containing the source of cardiac electrical activity at its center. Einthoven placed the electrodes at the top of an equilateral triangle at the center of which he imagined the heart to be there (Figure 6) [11].

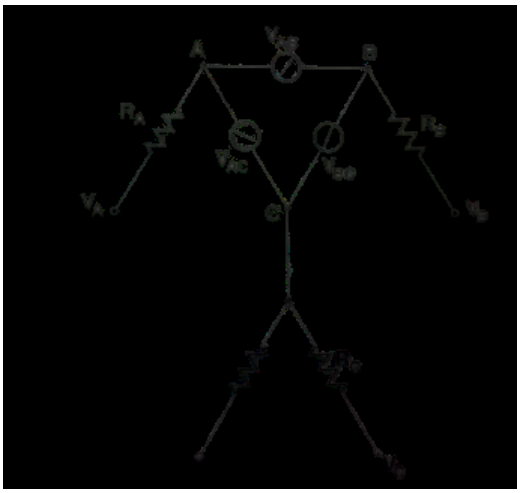

Figure 6. Equivalent circuit relating to the Einthoven triangle [11].

Einthoven indicated point A right arm, point B left arm, and point C the basis of the sternum. An arrangement of the electrodes thus provides the temporal trend of the projections of the vector H along three directions belonging to the frontal plane. Even if the position of the electrodes is not that indicated by Einthoven, i.e. for example the electrode B was allocated on the left wrist, the electrocardiographic trace would differ very little since the arms (and legs) behave like open circuits in the which does not flow any appreciable current induced in the presence of the dipole. It follows that the potential at their ends is equal to that of the points A, B and C respectively. It should also be noted that the three electrodes constitute the nodes of a mesh in which the first Kirchoff principle can be applied, i.e. it allows to deduce the value of a lead knowing the other two potential differences [11].

The triangle shown in figure 7b is called the Einthoven triangle and the places A, B and C are better identified respectively as RA (Right Arm), LA (Left Arm), LL (Left Leg). The straight lines joining RA with LA, RA with LL and LA with LL identify three directions respectively representable with three verses a_1, a_2 and a_3, which constitute an equilateral triangle for which the versor a_1 identifies the horizontal direction (from the right arm to the left arm).
The other two directions are defined accordingly. The projection of the vector H on the directions a_1, a_2 and a_3 identify scalar quantities V_1, V_2 and V_3 according to the relation [11]:

$$V_i = H \cdot a_i \quad \text{with } i=1,2,3 \tag{3}$$

Therefore, they are the scalar product between the heart vector H and the versors a_i. In particular:

- the potential difference between RA and LA, that is $V_{LA} - V_{RA} = V_1$, is named I lead;
- the potential difference between RA and LL, that is $V_{LL} - V_{RA} = V_2$, is named II lead;
- the potential difference between LA and LL, that is $V_{LL} - V_{LA} = V_3$, is named III lead.

The recording of these cardiac potentials is performed with a recorder millivoltmeter (electrocardiograph) for which, with respect to the reference potential called *isoelectric*, the displacement above this is indicated as positive and the opposite negative.

This circumstance occurs if the conventions of the signs of the polarity are respected those indicated in Figure 7 b and c. The isoelectric used as a reference coincides with the potential value of the right leg. Galvanometric recording on graph paper takes place with a standard speed of 25 o 50 $mm \cdot s^{-1}$. Each millimeter therefore represents 0.04 s or 0.02 s. The standard amplification is 0.1 $mV \cdot mm^{-1}$. For monitoring the used frequencies are included between 0.05 - 50 Hz, while for diagnostics the frequencies used reach up to 1KHz [11].

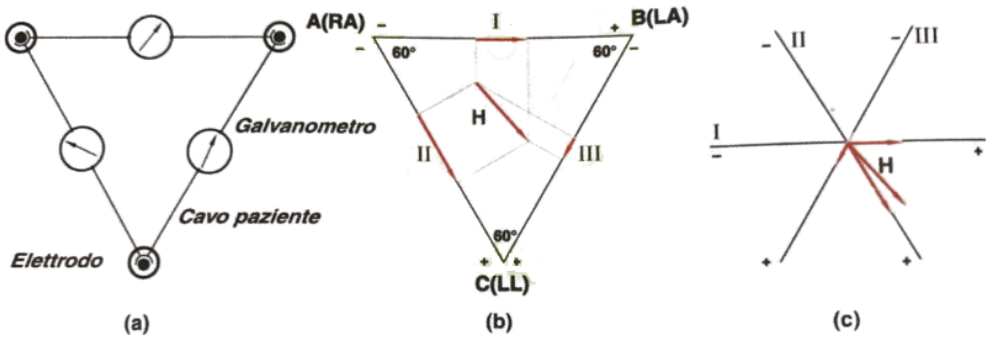

Figure 7. Einthoven triangle: bipolar standard leads. Connection circuit (a); heart vector H projection (b); triaxal reference system (c) [11].

The location of electrodes influences the recorded signal and produces a view of the heart from different angles (Figure 8). Therefore, each lead includes a specific information and a type of noise, which are different from the others. For this reason, it is useful to have multiple leads, that offers a complete view of the heart. Traditionally, the ECG is measured with three different lead systems: the aforementioned three bipolar leads (I, II and III), the six precordial leads (V1 –V6) and the three augmented unipolar leads (aV1 – aV3). These leads are collectively referred to as the standard 12-leads ECG configuration [12].

As already reported, the three bipolar leads are originated with fixed electrodes to the right arm, left arm and left leg. Together with the augmented limb leads they form the electrical frontal plane of the heart. The six precordial leads are measured by placing six electrodes directly on the chest for recording the potentials of the hearts electrical axis in the horizontal plane [12]. Figure 8 shows the different morphologies of the ECG signals in the 12-lead configuration.

When a depolarization wave front is moving towards the electrode a positive-value amplitude is observed in that lead (channel) and a negative one when moving away. Similarly, a repolarization wave front gives a negative-value amplitude when moving towards the electrode and so on. So according to the heart conduction system explained in the previous paragraph, the typical wave front constituting the ECG trace is shown in Figure 9 [13].

The P wave is caused by the propagation of the depolarization wave front during atrial depolarization. It appears upright in leads I, aVF and V3 - V6. Its polarity is positive in leads I, II, aVF and V4 - V6, diphasic in leads V1 and V3, and negative in aVR. P wave shape is generally smooth, not notched or peaked. The QRS complex is a result of ventricular depolarization and its amplitude is

greater than 0.5 mV in at least one standard lead, and greater than 1.0 mV in at least one precordial lead. Upper limit of normal amplitude is 2.5 - 3.0 mV. The last deflection is the T wave, which corresponds to ventricular repolarization. Its amplitude is of at least 0.2 mV in leads V3 and V4 and at least 0.1 mV in leads V5 and V6. Atrial repolarization occurs at approximately the same time as the QRS complex and is therefore invisible [13].

Normal values for waves and intervals are as follows:

- RR interval: 0.6-1.2 s
- P wave: 80 ms
- PR interval: 120-200 ms
- PR segment: 50-120 ms
- QRS complex: 80-100 ms
- ST segment: 80-120 ms
- T wave: 160 ms
- ST interval: 320 ms
- QT interval: 420 ms or less if heart rate is 60 bpm.

HRis the rate of the heartbeat measured by the number of contractions (beats) of the heart per minute. The heart rate varies according to the body's physical needs, including the need to absorb oxygen and excrete carbon dioxide. The American Heart Association states that the normal resting adult HR is 60-100 bpm [14].

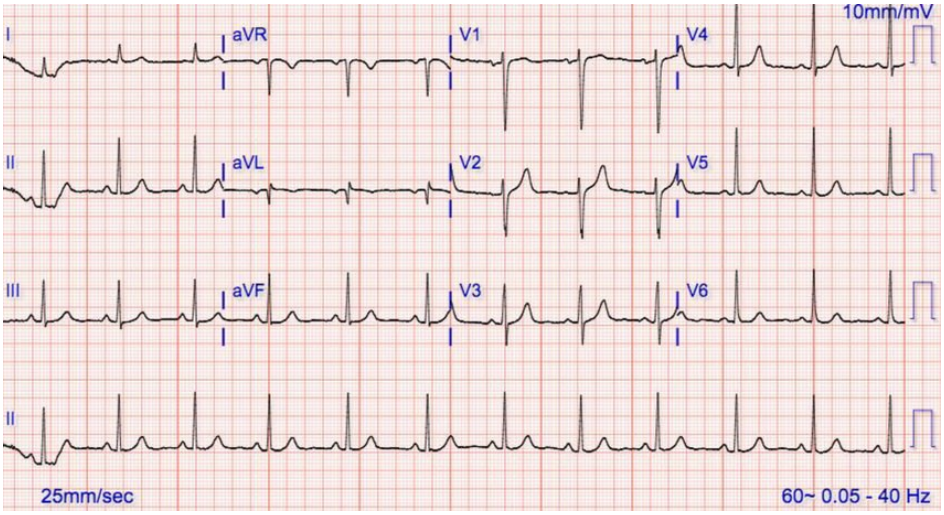

Figure 8. Normal sinus rhythm in the 12 leads of ECG.

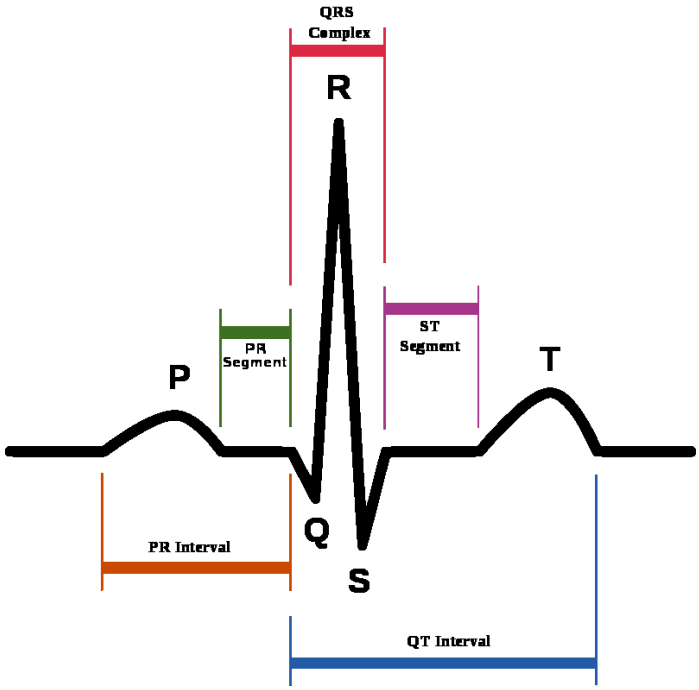

Figure 9. Electrocardiographic trace

1.2 Respiratory System

The respiratory system is composed of a set of hollow organs, the *airways*, and parenchymatous organs, the *lungs*. The lungs are the organs in which gas exchange between air and blood takes place, guaranteeing the intake of O_2 and the elimination of CO_2. From an anatomical and functional point of view, the respiratory system is therefore in close correlation with the cardiovascular system [10].

The breathing mechanism is considered from two perspectives, the first concerns the functionality of the system that transports oxygen from the inspired air to the cells and simultaneously discharges carbon dioxide from the cells to the air to be exhaled. This first perspective concerns the physiology of breathing, the problems relating to the acid-base balance and therefore pertains to diagnosis and therapy problems specific to the medical profession. The second perspective concerns the mechanical behavior of the lungs from a fluid dynamic point of view; it therefore has fundamental relevance in the design, control and maintenance of machines that are related to respiratory physiology and pathology [10].

The respiratory function is carried out in two phases: i*nspiration*, through which the air containing O_2 from the external environment and through the pathways areas reaches the lungs; the *exhalation* with which the air, loaded with CO_2, from the lungs retraces the airways in the opposite direction and is emitted to the external environment [10].

1.2.1 Anatomy of the respiratory system

The airways are channels that bring air from the external environment to the lungs and are represented by the *nose, pharynx, larynx, trachea* and *bronchi* (Figure 10) [10].

The nose has a skeletal part, the nasal pyramid, supported by bones of the facial mass (maxillary, nasal), by some cartilages and by muscle bundles of the furrier or mimic muscles. Air enters the airways (or respiratory tract) through the nostrils, then passes through the vestibules to access the nasal passages. The vestibules are covered with skin and have robust, rather long, hairs called vibrissae [10].

The nasal cavity, divided by the nasal septum, are located in the thickness of the jaws and have an anfractuous lateral wall due to the presence of the turbinates or cornets, which connect the air column with the cavities, or paranasal sinuses, which are located in the thickness of neighboring bones (frontal, maxillary, sphenoid). The walls of the nasal passages are lined with a respiratory mucosa, that is, provided with a vibrating epithelium, with cilia and mucus-secreting glands. The nasal mucosa has the function of retaining the atmospheric air and eliminating the atmospheric dust that arrives with the inspired air in the airways. In addition, mucus moistens the air, which reaches the lower airways saturated with water vapor. The rich vascularization of the mucosa, releasing heat, allows to heat the atmospheric air [10].

From the nasal cavity, the air passes into the pharynx, a channel in common between the respiratory and digestive systems [10].

At the end of the pharynx there are in fact the larynx, anteriorly, and the esophagus, posteriorly. During swallowing the transit to the larynx is prevented by the epiglottis. The larynx, in addition to allowing the passage of air, performs functions in the production of sounds. It is supported by a fibro cartilaginous scaffold, to which the thyroid, cricoid, arytenoid and cornicular cartilages contribute; it is then anchored to the hyoid bone by a set of fibro elastic membranes. The larynx has a remarkable musculature (intrinsic and extrinsic), with an extremely sophisticated possibility of reciprocal movements, so much so as to have allowed the human species to acquire the word. It is covered with respiratory mucosa, which at the level of the thyroid cartilage rises in two folds on each side: the upper pair is that of the false vocal cords, simple recesses; the lower one is formed by the true vocal cords. The glottis opens between the true vocal cords, which is the narrowest point of the upper airways [10].

The trachea departs from the cricoid cartilage, an organ placed in front of the oesophagus and consisting of a series of incomplete fibro cartilaginous rings on the posterior side, and held together by a fibrous tunic [10].

At the height of the fourth or fifth thoracic vertebra the trachea bifurcates and gives rise to the two main bronchi, which retain the trachea structure and share its coating, which consists of a respiratory mucosa, with ciliated lining epithelium and numerous mucous glands and serous. After penetrating the lung, the main bronchi soon divide into the lobar bronchi [10].

These successive branches, which form the so-called *bronchial tree*, are distributed throughout the lung parenchyma; up to the lung lobules the structure with incomplete fibro cartilaginous rings is preserved and this allows these "channels" not to close [10].

The lungs are two parenchymatous organs, contained in the thoracic cavity, divided by a space, the mediastinum, which houses the esophagus, trachea and heart. The base of each lung rests on the diaphragm; the curved side face is in contact with the ribs; the central face is precisely in relation to the mediastinum, and on it is the pulmonary hilum, that is the point of entry of the main vessels and bronchi. The right lung is larger than the left: in fact, the left the thoracic cavity also houses the heart. The right lung is divided into three lobes, the left lung into two, plus a pulmonary lingula. The lobes are separated by the infoldings of the pleura, called fissures. The lungs after birth have a high content of air, enough to float on the water [10].

The air is contained in the alveoli, very small spaces delimited by thin epithelium laminae, in whose interstice run the capillaries that depart from the last branches of the pulmonary arteries. In the alveoli, the inspired air is separated from the blood only by the thickness of the capillary walls and the cells of the pulmonary epithelium, which facilitates the gas exchange between the two compartments. The lung is not reached only by the pulmonary arteries that carry venous blood to allow for the proper exchanges of the gas exchange, but also by the bronchial arteries that derive from the thoracic aorta and carry arterial blood. The pleura is a serous membrane, which wraps around each lung and is made up of two sheets: one visceral, which covers the lung in each of its lobes, and one parietal, which instead covers the internal wall of the rib cage [10].

The *pleural cavity* between the two leaflets contains a liquid that facilitates the sliding of the lung during breathing [10].

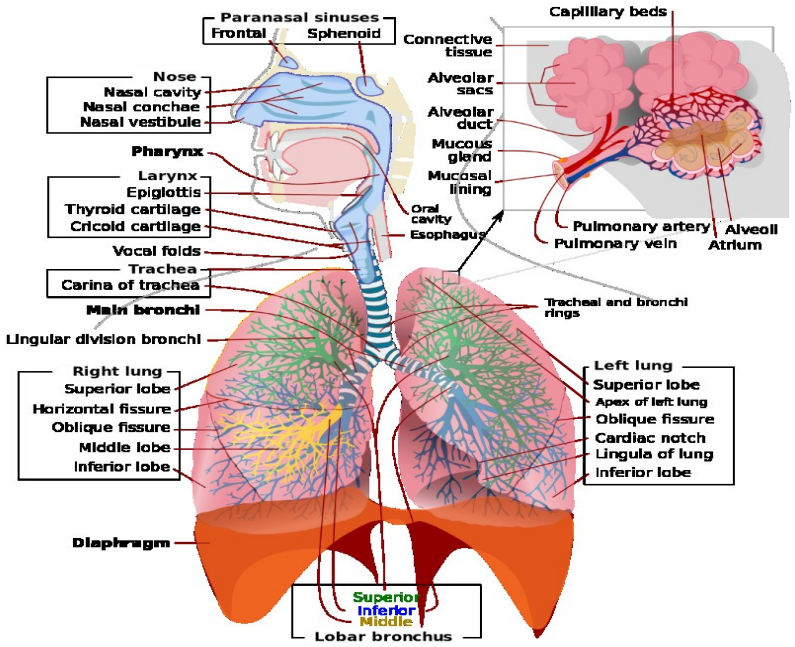

Figure 10. Respiratory System

1.2.2 Physiology of the respiratory system

The respiratory system can be assimilated to a volumetric container whose gas exchange is ensured by rigid, semi-rigid and elastic structures, which function as flow regulators. Furthermore, a distinction can also be made between internal and external respiration [10].

The first consists in the passage of oxygen from the blood to the cells and of carbon dioxide from the cells to the blood; the second consists in the exchange of oxygen and carbon dioxide between the blood that supplies the alveoli and the air contained in them. Schematically, the airways are divided into three sections arranged in series [10]:

- nose, whose cavities transform a turbulent air flow to a laminar one;
- the duct, which includes the larynx, pharynx and trachea;
- the bronchial tree, which ends with the alveoli.

Each alveolus is an elastic bag pervaded on one side by a bed of capillaries, where the blood flows from the arterial capillary to the venous capillary, while on the other side it is in direct contact with the inspired air. The lungs contain about 300 million alveoli in an adult and the lack of cartilage support in the lungs is remedied by the presence, in the very thin liquid film that covers the internal surface of the alveoli, of a lipid substance, the *pulmonary surfactant*. Its function is to vary the surface tension of the liquid that covers the internal wall of the alveolus, i.e. to vary the force generated by the mutual attraction between the molecules of the liquid surface. The pulmonary surfactant is in fact a surfactant, characterized by a surface tension that varies, moment by moment, during ventilation. The area of the alveoli surface, exposed to both capillaries and air, is approximately 40 times the body surface [10].

At the alveolar level, the gas exchange between air and blood is regulated by a passive process of physical diffusion; oxygen and carbon dioxide move from areas of greater concentration to areas of lower concentration. This diffusion is regulated by Fick's law:

$$\frac{dM}{dt} = \frac{A \cdot k \cdot (C1 - C2)}{s} \qquad (4)$$

which establishes that the mass of gas that diffuses in the unit of time (dM / dt) is proportional to the area of the exchange surface (A), to a diffusion constant k, to the difference in concentration (C1-C2), and inversely proportional to the thickness of the alveolar wall (s). To have a high perfusion A must be as large as possible and s as small as possible [10].

External breathing is carried out with the following mechanism: the oxygen of the inspired air, i.e. of the air that has reached the inside of the alveoli, is at a partial pressure pO_2 of about 150 mmHg, passes through the thin membrane in the venous capillary, where oxygen is at a partial pressure of about 40 mmHg. Carbon dioxide, which in the inspired air is at a partial pressure of about 0.3 mmHg, in venous blood is at a partial pressure of about 45 mmHg. Therefore, there is the passage of oxygen between the alveolar cavity where the pO_2 is greater and the lumen of the capillary where the pO_2

is less. The reverse occurs in the case of carbon dioxide. In conclusion, the pressures of oxygen and carbon dioxide in the blood and alveolar air balance quickly [10].

The gas exchanges in the lungs concern two different physiological processes:

- the one concerning the spraying of the capillaries, which is called perfusion;
- that concerning the circulation of air in the alveoli, which is called ventilation.

If one of the two processes become insufficient, the blood cannot be properly oxygenated. Internal breathing is also regulated by partial pressure ratios. In fact, once the exchanges in the lung have occurred, the arterial blood contains oxygen with high pO_2 and carbon dioxide with low pCO_2, while in the tissue cells there is exactly the reverse situation. These conditions establish pressure gradients that carry out the gaseous exchanges between blood and tissues. The transport of oxygen in the blood occurs thanks to a particular protein, hemoglobin. It is present in red blood cells. Hemoglobin binds chemically with O_2 molecules, forming oxyhemoglobin. An important parameter is defined that is capable of providing information on the efficiency of the transport of oxygen in the blood: oxygen saturation, SaO_2 [10].

The amount of carbon dioxide in the blood is of considerable importance as regards the acid-base balance of body fluids (blood pH), on which, among other things, the regulation of heart and lung rhythms depends. The chemoreceptors, located in the sinuses of the carotid arteries and on the aortic arch, are stimulated by the variation of the pH in the blood (depending on the variations of the pO_2 and pCO_2). The increase in arterial pO_2 stimulates the aforementioned receptors in order to reduce respiratory activity, on the contrary the increase in pCO_2 produces a stimulation that increases the frequency and depth of breathing [10].

Air enters the lungs because the diaphragm contracts and lowers and therefore offers more space for the expansion of the lungs in the lower part, while the intercostal muscles contract by moving the ribs upwards and outwards. This increase in the volume available to the lungs produces a reduction in intra pleural pressure, with a consequent decrease in alveolar pressure below atmospheric pressure. This allows external air, which is at atmospheric pressure, to enter the lungs. This generates an air flow inside the respiratory system which ceases as soon as the alveolar pressure returns to equilibrium with the atmospheric pressure. The exhalation phase is a passive phenomenon: the muscles of the diaphragm and the intercostal ones, relaxing, decrease the lung space, forcing the air that has entered to come out. The pleura is necessary to allow the lungs to move along the fixed wall (rib cage) without friction [10].

The amount of air introduced and expelled from the lungs essentially depends on three fundamental mechanical quantities that, individually or combined with each other, provide the physiological or pathological state of the respiratory system. These quantities are volume, flow and pressure. The volume is defined as the space that accommodates the air, considering the change produced by the diaphragm, intercostal muscles and lungs. By flow we mean the temporal modalities with which the air is introduced or expelled from the lungs, i.e. the speed it takes in the different phases of the respiratory cycle. Flow is meant the temporal modalities with which the air is introduced or expelled

from the lungs, i.e. the speed it takes in the different phases of the respiratory cycle. The pressure considered is that which is established in the intra pleural space, in the alveoli and in the upper airways [10].

1.2.3 Respirogram

The following graph (Figure 11) shows four normal breathing cycles of a healthy subject: inhalation (top lines), exhalation (bottom lines) and automatic pause (almost horizontal lines) accompanied by relaxation of all respiratory muscles. The abbreviation MV indicates lung ventilation and is the volume of air that can be inhaled or exhaled for one minute. The calculation of lung ventilation is simple: MV = VT * RF, or the product between the tidal volume (VT) and the RF [15].

During a normal respiratory activity, the characteristic parameters of the entire respiratory cycle are analyzed, the values of which are shown below:

- inspiration (1,5-2 s);
- expiration (1,5-2 s);
- automatic pause (2 s);
- tidal volume- inhalation depth (500-600 ml);
- respiratory rate or RF (10-12 breaths/min).

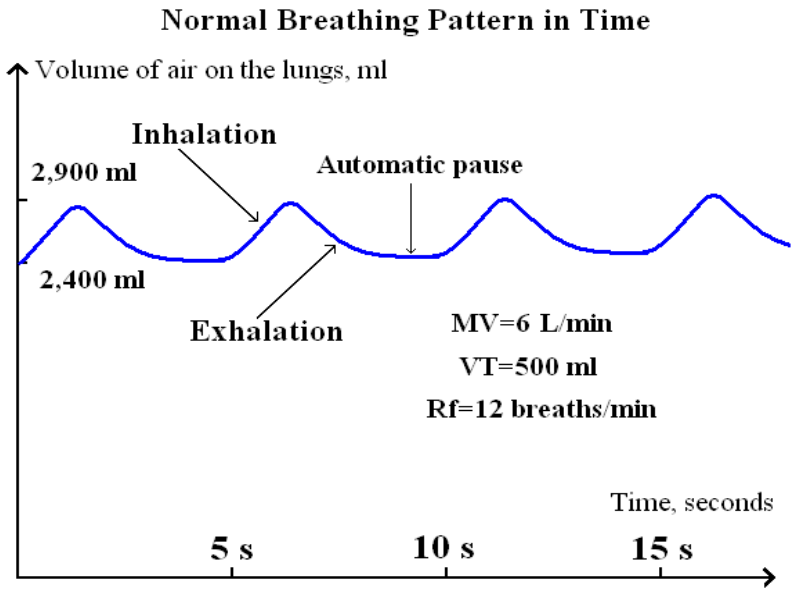

Figure 11. Normal Breathing Pattern in Time [15]

On average, an adult, in resting conditions, breathes (or, more correctly, ventilates) about 6/8 l of air per minute, that is, the same volume of blood that, in the same time, is pumped from the heart [15].

Respiratory frequency is defined as the number of breaths a person takes during one minute. It is usually measured at rest while the subject sits. The first data available on spontaneous respiratory rate values are those of Quetelet (1842) on 300 subjects and Hutchinson (1850) on 1714 adult subjects [15]. These data show the wide range of breathing rate (between 6 and 31 breaths per minute or between 0.1 and 0.5 Hz) observed in adults. In addition, they have the merit of being obtained from an observation and therefore not be altered by the use of any measuring device. RF changes with age, gender, weight; for example, in children it is higher than the values found in an adult. Table 1 shows RF typical values in the different phases of life. The wide range of RFs in resting human subjects has led to the search for an optimal breathing rate value.

RF may highlight some problems related to lung dysfunction. In fact, breathing accelerates, giving rise to increased frequency in patients when their health conditions are becoming critical [15].

The duration of inspiration and exhalation introduces an additional factor of diversity in breathing. For a given duration of the respiratory cycle (Ttot) there is a different combination of the times of inspiration (Ti) and expiration (Te), but in any case there is the constraint that Ti is lower than Te.

Another parameter to consider is the tidal volume, or the quantity of air that is mobilized with each non-forced respiratory act. The range of VT observed in resting human subjects varies between 442 and 1549 ml.

There are numerous methods for monitoring respiratory activity. A plethysmogram is a signal that gives a measure of changes in chest and/or abdominal volume recorded by a respiratory belt [16].

There two primary methods of non-invasive chest and abdominal plethysmography, which are based on different kinds of sensor fixed to a long hook and loop strap that is placed around the chest or abdomen. Optionally, in some application a second respiration sensor is placed around the chest for helping abdominal breathing recording. So according to the integrated sensors, there are measurement of changes in elastic belt tension and measurement of changes in electrical inductance [16].

Table 1 RF typical values [15]

AGE	Respiratory Frequency (Breaths Per Minute)
New born	30-60
Infant (1 to 12 months)	30-60
Pre-Schooler (3-5 years)	22-34
School-age child (6-12 years)	18-30
Adolescent (13-17 years)	12-16
Adult	12-18

By using elastomeric plethysmography, an elastic belt will exhibit a change in tension as the chest or abdomen expands or contracts. This change in tension can be easily measured and converted to a voltage by a variety of methods. The most common is through piezo-electric sensor, i.e., a crystal that directly generates a voltage when compressed or stretched. This resistive belt has the disadvantage that all types of movements, as turning of the torso, will cause spike wave distortion in the piezo; for this reason, it is more sensitive to movement artefacts compared with the others. The resistive belts have signals with lower amplitude and more noise, but they are cheaper and easier in use [16].

In respiratory inductance plethysmography, an elastic belt into which a coiled wire is sewn (to allow for expansion and contraction) is worn around the chest or abdomen. An alternating current (AC) is passed through the belt, i.e. a loop of wire, generating a magnetic field normal to the orientation of the loop (Faraday's Law). The frequency of the alternating current is set to be more than twice the typical respiratory rate in order to achieve adequate sampling of the respiratory effort waveform. The act of breathing changes the cross-sectional area of the patient's body creating an opposing current within the loop directly proportional to the change in the area (Lenz's Law). This opposing current can be measured through changing in the frequency of the applied current and it represents an accurate representation of the change in cross-sectional area. The signal from inductive belt always has a large amplitude and are rather stable in relation to movement artefacts, because it does not rely on belt tension. Figure 12 shows the respiratory inductance plethysmography signals extracted from two belts on the chest and abdomen; they are used to obtain indirectly other respiratory information as the respiratory rate and tidal volume [16].

Figure 13 shows a belt respiration signal, where the cycles of respiration are clearly visible. The signal reflects the sinusoidal profile of the respiration.

Sensors positioned at different trunk heights can also be used, in particular to discriminate between respiratory activity at the thoracic level and respiratory activity at the abdominal level. The response of these sensors was assessed through a comparison and the two signals show similar morphologies and coincident respiratory rate values. Despite movement artefacts, thoracic and abdominal activity can be discriminated against, as can be seen in Figure 14. From the Figure, it is possible to note that the phases of the abdominal and thoracic breath are opposite, in the experiment the paradoxical breath was simulated (with each inspiratory act the abdomen expands while the thorax narrows and vice versa) [16].

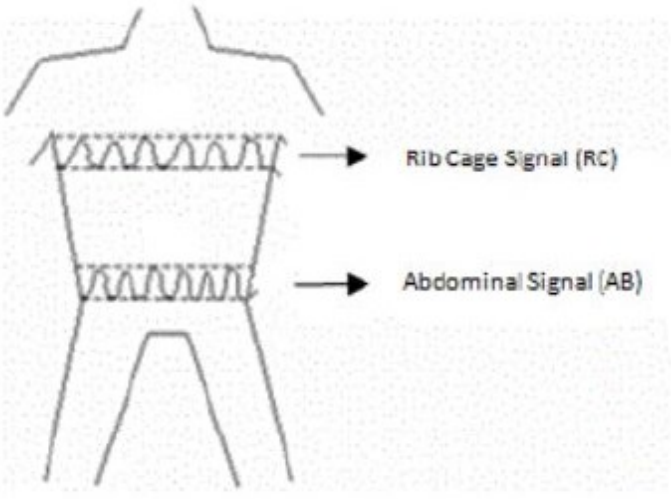

Figure 12. Dual band respiratory inductance plethysmograph with bands on torso [16]

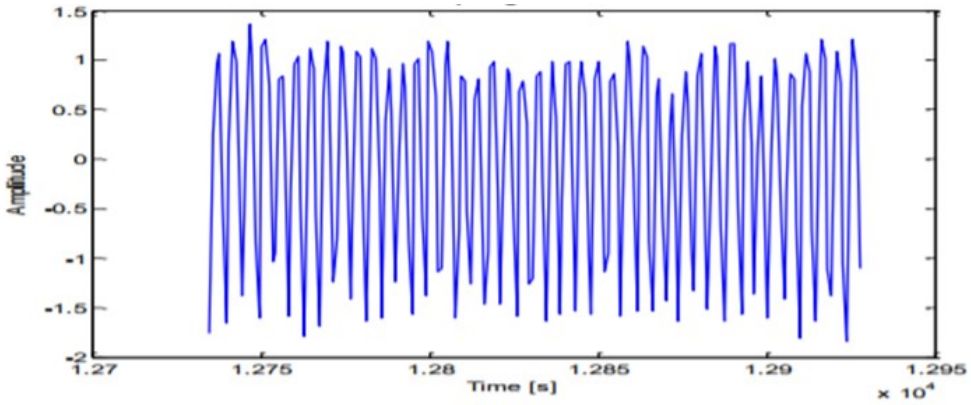

Figure 13. Example of respirogram

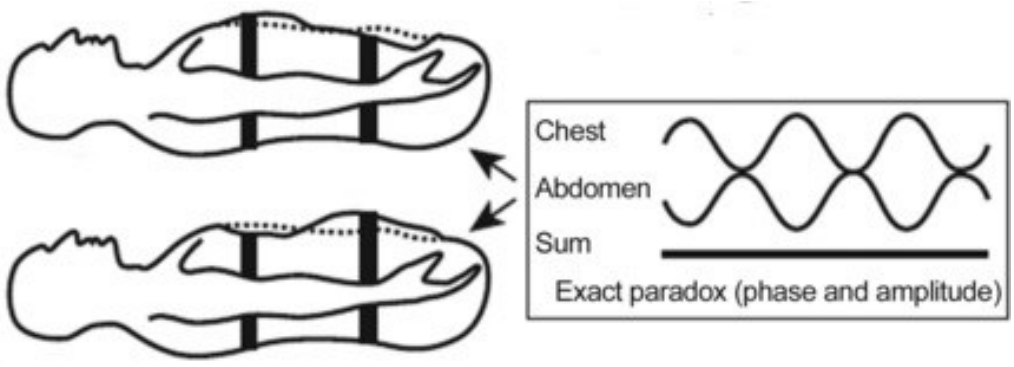

Figure 14. Chest respiration (above) and abdominal respiration (below), paradoxical breathing was simulated during the acquisition.

Chapter 2: Extraction of the respiratory signal from the electrocardiogram

2.1 Respiratory Modulation of the electrocardiogram

It is now recognized that there are characteristics related to breathing within the ECG signal. Specifically, the ECG shows three modulations due to the respiration: baseline wander (BW), amplitude modulation (AM), and frequency modulation (FM) (Figure 15) [17].

One or more of these modulations are analyzed by the algorithms in order to estimate the RF. The three dominant effects of breathing on the ECG can be summarize as follows. Changes in the orientation of the heart's electrical axis relative to the electrodes and changes in the thoracic impedance are the main causes of BW and AM. The variation of the electrical vector related to the respiration arise from filling and emptying of the lungs and from respiration-induced displacement of the heart. Changes in the impedance distribution occur due to the air flowing through the lungs, whereas the diaphragm movements provoke the cardiac shift. During inspiration, the apex pf the heart is stretched towards the abdomen because of the filling of the lungs, helped by the shifting down of the diaphragm. During expiration, the elevation of the diaphragm, for emptying of the lungs, compresses the apex of the heart toward the breast. Therefore, respiration induces a modulation of the heart electrical axis since it changes the angle that the electrical cardiac vector makes with a reference line [17].

Instead, FM is due to a spontaneous increase of the heart rate (HR) during inspiration, and decrease during exhalation. This last modulation is also known as respiratory sinus arrhythmia (RSA).

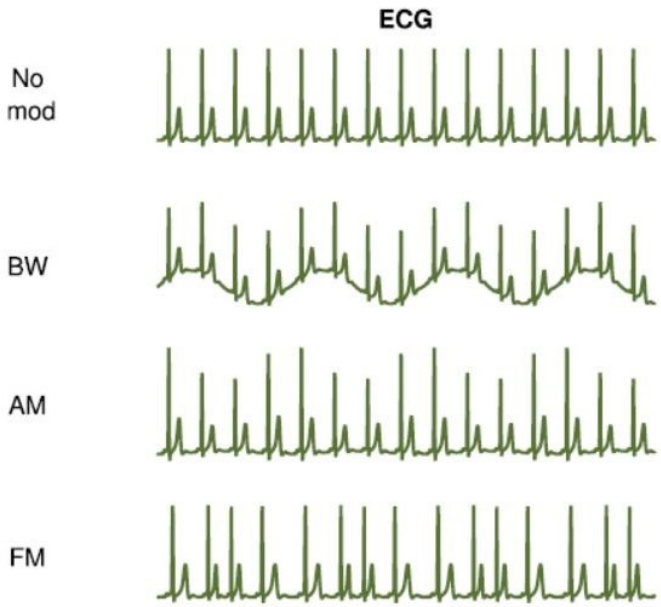

Figure 15. ECGs showing the three respiratory modulations compared with a no modulated ECG: baseline wander (BW), amplitude modulation (AM), and frequency modulation (FM) [17].

The three dominant effects that cause RSA are reported below [17]:

1. the sinoatrial node is stretched by changes in intrathoracic pressure during inspiration, increasing HR;
2. vagal outflow is increased during exhalation, reducing HR;
3. left ventricular stroke volume is decreased due to the reduced intrathoracic pressure during inspiration. This will cause a baroreflex-mediated increase in HR.

The force of these modulations can vary by considering different patient or subject groups. In fact, significant variations among subjects have been reported [1]. Moreover, some of these modulations may decrease in a specific population. For example, a decrease in FM is observed in elderly subjects. For these reasons, the RF algorithms that analysed multiple modulations provide a better performance [17].

Many algorithms have been proposed to estimate the RF from the ECG and a review of the literature is reported in order to identify the main characteristics of these algorithms. For gathering articles different databases or online libraries were used: Google Scholar, IEEE *Xplore*, PubMed, Science Direct, and Scopus. The first publication dates back to 1971, and nine publications were released between 1971 and 1998. Since 1999, the rate of publication has increased and nowadays this rate is of 20 publications each year. This trend demonstrates a higher interest in the topic and in the RF algorithms [17].

2.2 Respiratory Frequency Algorithms

Respiratory frequency algorithms may be thought as structured in 5 steps (Figure 16) [17].

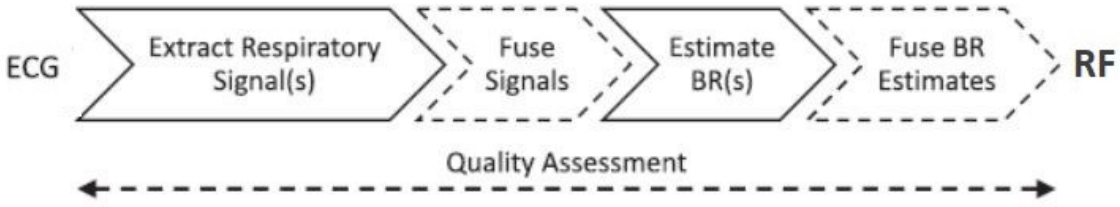

Figure 16. Steps of a RF algorithms. The steps represented with a dashed line are facultative [17].

The steps can be described as follows:

1. *Extract Respiratory Signal(s)*: extraction of one or more signals in which the respiratory modulation is present;
2. *Fusion of Respiratory Signals:* the analyzed respiratory signal can be obtained by the fusion of multiple respiratory signals (facultative step);
3. *Estimate RF(s):* estimation of RF from a window of the respiratory signal;
4. *Fuse RF(s):* an estimate of the RF can be obtained by the fusion of multiple RFs (facultative step);
5. *Quality Assessment:* it used to exclude imprecise estimates (facultative step).

2.2.1 Extraction of the Respiratory Signal

The first step consists in the extraction of a signal influenced by respiratory modulation from where the RF may be easily estimated (Figure 17). The most common signal used for this purpose is the ECG, but also other signals can be used, such as the photoplethysmogram signal (PPG).

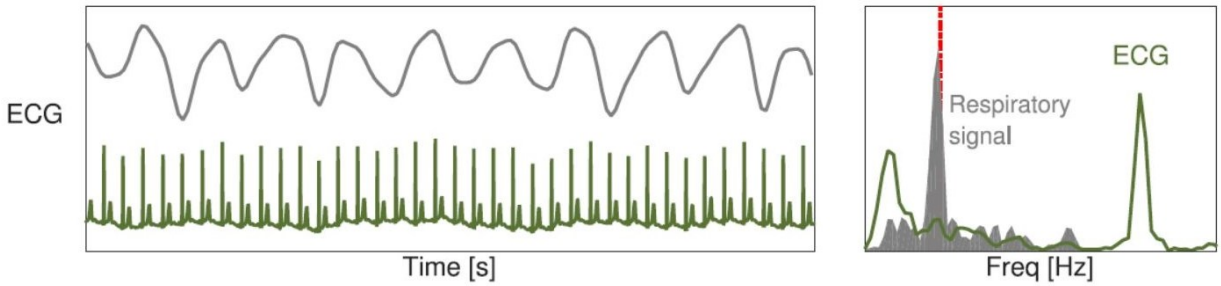

Figure 17. Extraction of respiratory signal: ECG and its derived respiratory signal depicted on the left. On the right the corresponding frequency spectrum is shown. The frequency spectrum of the raw ECG is dominated by cardiac frequency content at 1.2 Hz. In contrast, the extracted respiratory signal is dominated by respiration at 0.3 Hz, which is approximately the RF provided by a reference respiratory signal (shown by the dashed line) [17].

Two main techniques for the extraction of a respiratory signal can be distinguished: feature based or filter based techniques [8]. In feature-based techniques, the extraction of beat-by-beat feature measurements is performed (e.g., the QRS complex amplitude). Filter based techniques provide for raw signal filtering in order to attenuate non respiratory frequency components. The individual processing steps used in the extraction of the respiratory signal can be explained as follows [17]:

1. *Elimination of very low frequencies*: in this step the very low frequency (VLF) components of the ECG are removed, i.e. those at sub-respiratory frequencies. VLF components are eliminated through high-pass filtering using: a median filter; subtraction of the baseline trend calculated using a linear or polynomial fit; or measurements of the baseline at a specific point in the cardiac cycle (e.g., shortly before the QRS complex, or at midpoints between successive R waves in the ECG). The cut-off frequency is usually set between 0.03 and 0.05 Hz. This step is recommended regardless of which technique is used.
2. *Feature-Based Techniques*: these techniques include several phases to extract a time series of beat-by-beat features. Figure 18 shows examples of the used feature-based technique. Initially, there is the elimination of the of very high frequency (VHF) noise by low-pass filtering to improve the accuracy of the beat detection and feature measurements. In order to preserve the high frequency content of the QRS complex, high cut-off frequencies are used. Moreover, since the ECG is particularly susceptible to power-line interference, a band-stop filter can be also used to delete it.
   Then, individual beats and their fiducial points are identified (i.e., Q- and R- waves). These fiducial points are used to measure a feature that changes with the respiration. The identified fiducial points and their derived feature measurements are specific to the particular feature-based technique used (Table 2). Differences in the feature-based techniques can be observed, such as the use of multi-lead ECGs or non-standard leads derived from them, for example.

Usually, the signals obtained from beat-by-beat feature measurements are irregularly sampled (once per beat). Since the subsequent processing often requires a regularly sampled signal, the time series of the beat-by-beat feature measurements is resampled at a regular sampling frequency that ranges between 4-10 Hz. In most cases, a linear or cubic spline interpolation is used.

3. *Filter-Based Techniques*: The extraction of the respiratory signal by using these techniques are performed in a single step. A general approach in the case of BW modulation may be the use of a band-pass filter to remove frequencies outside the plausible range of respiratory frequencies. Instead, in the case of AM and FM modulations, the filter-based techniques may involve the use of the continuous wavelet transform. The different approaches found in literature are reported in the Table 3.
4. *Elimination of Non-Respiratory Frequencies:* In order to avoid the wrong identification of spurious frequency content as the RF, non-respiratory frequencies should be removed from the respiratory signal. For this purpose, a band-pass filtering may be used, with cut-off frequencies at either end of the range of plausible respiratory frequencies. However, there are discrepancies about what it is this optimal range. Moreover, the range should be adapted according to the considered population, especially for children. As a guideline, Karlen *et al.* used a range of 4–65 breaths per minute [18].

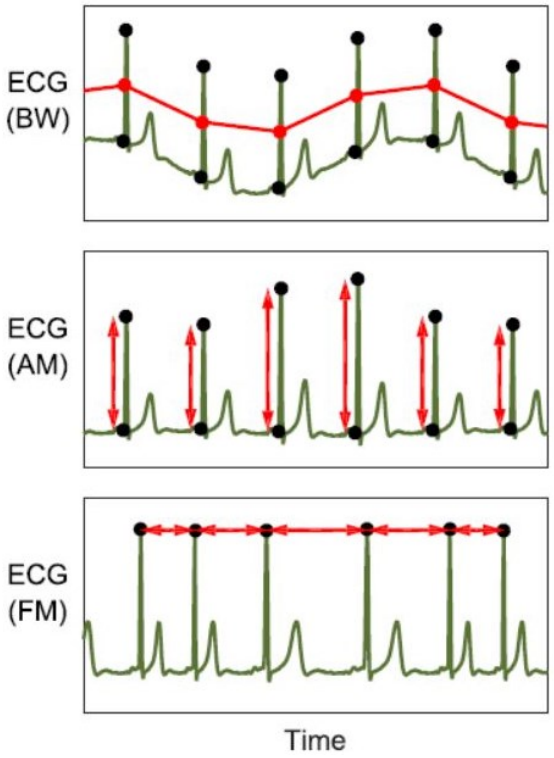

Figure 18. Examples of feature-based techniques for the extraction of the respiratory signal form the ECG: measurements of baseline wander (BW), amplitude modulation (AM), and frequency modulation (FM) have been extracted for each beat from fiducial points (shown as dots) [17].

Table 2 Feature-Based Techniques for the Extraction of Respiratory Signals [17]

• The mean amplitude of peaks and preceding trough or the mean signal value between two consecutive troughs is used to extract BW [19,20] • The difference between the amplitudes of the peaks and preceding troughs are used to extract the AM [21] • Time interval between consecutive peaks to extract FM [21] • Extract peak amplitudes [22]. • Extract trough amplitudes [20] • PCA of heartbeats [21,23] • Extract the morphological scale variation of the QRS complexes or other part of the signal by comparing the considered beat to a template one [24] • Extract QRS durations [25] • Extract QRS areas [26] • Extract the maximum Q-R or R-S slopes [27] • Extract the direction of the electrical heart vector at a specific phase in the cardiac cycle (e.g., T wave) [28]

Table 3 Filter-Based Techniques for the Extraction of Respiratory Signals [17]

• Band-pass filter to remove frequencies not included in the plausible range of respiratory frequencies [17] • Use (ensamble) empirical mode decomposition to extract a respiratory signal as either one particular oscillation mode (intrinsic mode function, IMF) or the sum of the IMFs indicative of respiration [29] [17] • Reconstruction of the respiratory signal by decomposing the original signal through the discrete wavelet transform [30] [17] • Extraction and processing of the EMG signal from high-frequency content of the ECG caused by the activation of the diaphragm and intercostal muscles during respiration [31].

2.2.2 Fusion of the Respiratory Signal

In this second step a single respiratory signal can be obtained through the fusion of multiple respiratory signals in order to estimate the RF. Multiple respiratory signals can be obtained by extracting multiple signals at the same time (e.g., by using different extraction methods or by using both the ECG and another signal such as PPG) or by divided a respiratory signal into several (often overlapping) windows and treating them as individual signals. This step is facultative and is used to increase the accuracy and robustness of the estimated RF. This step is useful especially in presence of significance motion artefacts, such as during exercise [17].

2.2.3 Estimation of Respiratory Frequencies

The third step consists in the estimation of RF. This step has as input a window of the respiratory signal and the output is a RF estimate. Several techniques operating in both time and frequency domain are used. Time-domain techniques have the advantage of not requiring a quasi-stationary RF although they are susceptible to spurious breath detection due to abnormal respiratory signal morphology. Frequency-domain techniques involve identifying the frequency component related to respiration, typically through spectral analysis or identification of the instantaneous dominant frequency. One of the most common approach is the spectral analysis and the use of the fast Fourier Transform, where the RF is individuated as the frequency corresponding to the maximum spectral power in the range of plausible respiratory frequencies. Usually, this is the last step for most of the RF algorithms [17].

2.2.4 Fusion of the Respiratory Frequencies

The robustness of the final RF estimate may be improved by fusing several RF estimates. Several techniques may be used to fuse RF estimates obtained from different respiratory signal. RFs can be fused by averaging using the mean, median, or mode after the outliner exclusion. The standard deviation of the individual estimates may be used to assess the quality of the final estimate. Otherwise, the fusion of the RFs may be provided by weighting them considering their variances. Another approach may include the use of a Kalman filter, where RFs are weighted according to confidence metrics [17].

2.2.5 Quality Assessment

This last step is optional and may include two main types of technique: signal quality indices (SQIs) and respiratory quality indices (RQIs) [17].

SQIs method identifies the low quality ECG segments. For low quality is meant a segment of signal rejected on the basis that the derived estimation of RFs will not be accurate. This method works by considering the correspondence between the signal and a template, which is constructed computing the average of the beat morphology, and the calculation of the correlation coefficient between individual beat and the template. A part of the signal is considering of high or low quality by the comparison of the average correlation coefficient for that segment with an empirically determined threshold [17].

RQIs evaluate the quality of respiratory signals considering the regularity of the breathing peaks and the periodicity of the respiratory waveform. In order to do this both frequency and time-domain techniques are used: Fourier Transform, auto-regression, statistical analysis of the variations in the respiratory peaks, autocorrelation, etc [17].

2.2.6 Example of the Respiratory Frequency Algorithms

In more details, examples for each type of RF algorithm are reported and described.

Feature-Based Technique Examples:

In Helfenbein et al. paper [31] two examples of the feature-based technique are described.

Their first method is based on QRS axis shifts that are produced by changing the cardiac vector projections onto a changing electrode geometry which occur when the lungs are filled with air. Beats are detected by using a QRS detector. The total QRS amplitude is measured as shown in Figure 19. At each beat, the QRS amplitude is used as the respiration signal amplitude (circles on the lower plot in Figure 19). The EDR is obtained through cubic interpolation. In the last step, the EDR is filtered with a band-pass filter, where the cut-off frequencies are suitable for the plausible respiratory frequency range. A pro of this method is that the QRS detection and measurement are resistant to muscle artefact. A disadvantage of this kind of method is that obstructive apnea episodes can be missed if the QRS axis shift is present due to the respiratory effort and chest movement but without airflow. Another drawback is that the respiratory wave samples are obtained only at QRS times, and there is the risk that the signal is under-sampled if the HR is low or respiration rate is high; the accuracy depends on the cubic splines.

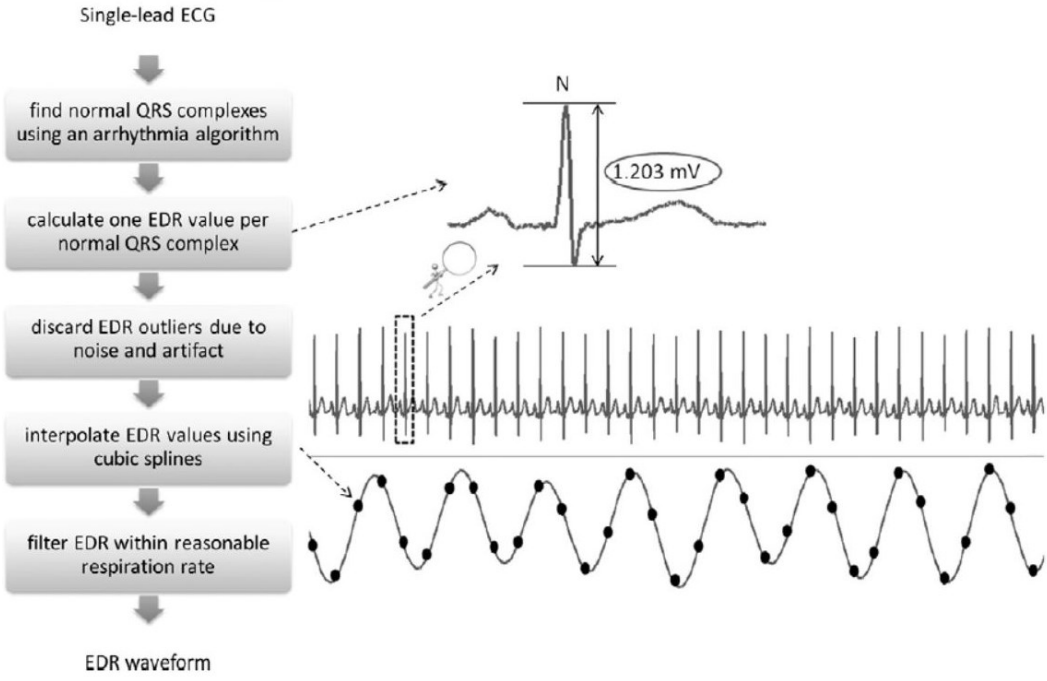

Figure 19. Block scheme of the method used for the extraction of the EDR from single-lead ECG. Peak-to-through QRS amplitude (EDR value) is measured for each normal QRS complex. Outliners (SD >2 from the mean) are excluded. The obtained values are then interpolated through cubic spline. The EDR signal is filtered with a band-pass filter [31].

In their second method, Helfenbein et al. consider the instantaneous HR (IHR) variability provoked by the RSA. As already explained, the HR changes in the two phases of the respiration: it increases during the inspiration and decreases during the exhalation. As shown in the Fig. 20 the R-R interval is used to compute the variability of the IHR, defined as the inverse of the R-R. Then, the IHR value

is used as the respiration wave amplitude at each beat (illustrated in the Figure 20 as the height of the arrow). The EDR is obtained also in this case by using a cubic interpolation. Since only the location of the QRS complex is necessary, also this method is particularly resistant to muscle artefacts. A drawback is that the RSA naturally decreases in elderly subjects or in the presence of particular diseases; for this reason, the method provides good results in a part of the population (e.g., healthy and young subjects). As for the previous method, only at QRS times the respiratory wave samples are available, hence the respiratory signal can be under-sampled and it is dependent on the accuracy of the cubic spline. However, these techniques based on HR cannot be used in case of atrial fibrillation, where the RR intervals are irregular and so they do not contain any respiratory information [31].

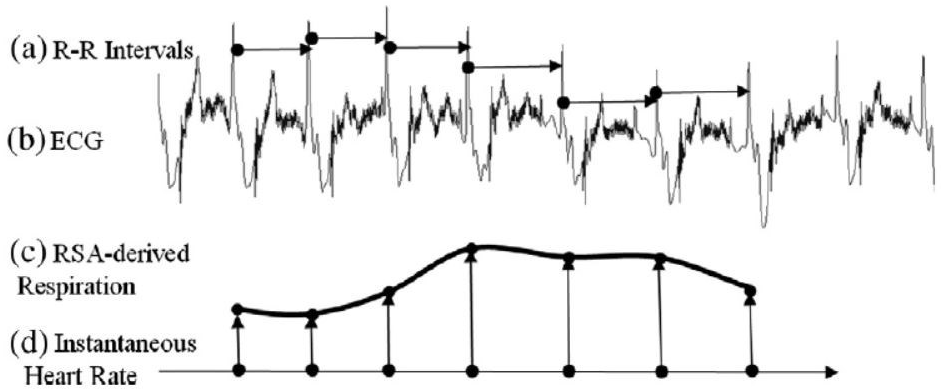

Figure 20. R-R interval ((a) horizontal arrows) variation identified from the ECG (b). The inverse of the R-Rs ((d) vertical arrows), calculated as instantaneous HR, are used as amplitude knots for the cubic interpolation to create the EDR signal [31].

Filter-Based Technique Example:

According to Santo et al. paper [32] respiration may be extracted from single-lead ECG through Discrete Wavelet Transform method. This method consists in the decomposition of the total signal into two components by using low-pass filters (LPF) and high-pass filters (HPF) (Figure 21). The obtained components contain half of the original information. LPF Coefficients are indicated as 'approximation' and HPF Coefficients are indicated as 'details'. In this case, the ECG must be decomposed enough levels until the lower frequency contents related to the respiratory signal are observed in the discrete wavelet transform coefficients. In this study, the ECG is decomposed with the discrete wavelet transform up to 9^{th} level or 10^{th} level in order to get a waveform similar to the respiratory signal. The bandwidth of these decomposition levels is below 0.46 and 0.23 Hz, respectively. Considering that the mean RF in an adult is 0.2 Hz, which correspond to 12 breaths/min, it is an acceptable frequency range. In the second phase, a single level is reconstructed through the high frequency reconstruction filters of the discrete wavelet transform, removing the coefficient 'approximation' (low frequencies) components. After obtaining the coefficients 'details' (high frequency) reconstruction, a threshold is applied and a peak detection algorithm is used. The outcome is interpreted as individual respiration movement, from which the RF is estimated (Figure 22).

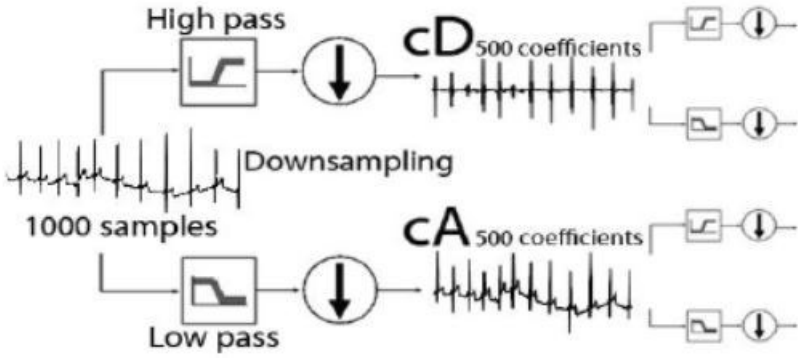

Figure 21. Discrete Wavelet Transform Decomposition Method [30]

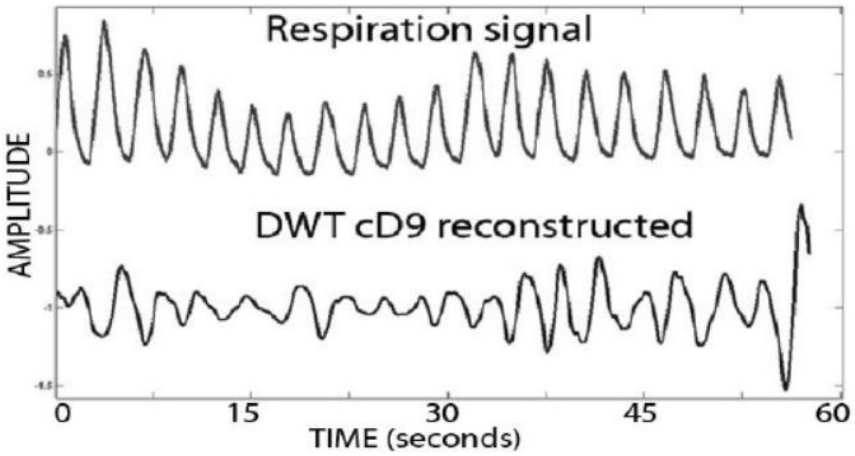

Figure 22. Comparison between the respiration signal and the reconstructed one. DWT: discrete wavelet transform; cD9: coefficients 'detail' up to the 9th level [32].

2.3 Assessment Methodologies Used in the Literature

In literature, a higher interest is addressed in the development of new RF algorithms rather than comparisons of already existing algorithms. The assessment of the algorithm performances proposed in the different publications is made difficult by several issues. These issue are: the use of different statistical measures, the use of data from different subject populations, and the lack of standardized implementations of algorithms. In addition, some methods are very accurate during sleep studies, whereas others are proved to be robust during stress testing, so the choice of a particular algorithm depends on the application. For all the above listed reasons, it is not possible to establish which algorithm performs best [17].

In literature, most of the papers propose the ECG as the input signal, but also other signals can be considered (PPG) [17].

There are advantages and disadvantages to the use of shorter and longer window durations with RF algorithms. The most common duration ranges between 30 and 90 s, however duration between 5-300 s have been used [33, 34]. Some studies have evaluated the performance of these algorithms considering the used window duration [18, 35]. These studies highlight that there is a (non-significant) trend toward lower errors at longer window durations. However, there are discrepancies

about what it is the optimal window length, because it seems to differ according to the considering populations and applications. The required time to measure RF and the computational requirements of RF algorithm decrease in the case of shorter windows. There is also a higher probability that the RF is more stable throughout the window. Moreover, RF can be tracked more precisely. Both these two latter conditions are preferable during exercise. On the other hand, the accuracy of the algorithms and the range of detectable RFs is increased with the use of longer windows. A good compromise seems to be a duration of 32 s [18].

In some cases, the databases used in these publications were not representative of the target population and not publicly available [17]. This wide range of used databases make difficult to assess in an objective way the algorithm performances.

Usually, the RF estimates are compared with reference RFs, which are estimated by using several techniques. Typically, a respiratory signal was acquired from which reference RFs were estimated using a bespoke algorithm. Many bespoke algorithms were used although often there was no assessment of their performances. This makes difficult to know whether errors in RF estimates derived from the ECG were due to the RF algorithm performance or contributed to by inaccuracies in reference RFs [17].

The performance of RF algorithm is evaluated by using a wide range of statistics. Statistics were most commonly calculated from the errors between reference and estimated RFs, including the mean (absolute) error, root-mean-square error, and the percentage error. The LOAs method, consisting of the systematic bias and LOAs within which 95% of errors are expected to lie, was used less often. This method is useful because certain applications require greater accuracy (such as identification of pneumonia indicated by RF > 40 bpm [18]), whereas others require greater precision (such as detection of acute changes in RF indicative of deterioration [19]). Correlation coefficients were used in a minority of publications [17].

In conclusion, several RF algorithms from ECG are reported in the literature. Most of them have a standardize structure, where each stage has many different mathematical techniques. Now, clinical devices incorporate RF algorithms and this aspect encourage the study of their performance and utility in both hospital and the community. Further work is required to identify the most suitable RF algorithms for use in different settings and to determine how RF algorithms can be used to deliver patient benefit [17].

Chapter 3: Extraction of the respiratory frequency from the electrocardiogram

3.1 Materials and Methods

3.1.1 Clinical Data

The clinical data used in this study was collected and provided by Università of Rome Foro Italico. Data was collected from nine healthy male subjects (mean age± SD: 45.2± 8.6 years).

The protocol of the experiment provided that the subjects were involved in a graded exercise test on a cycle ergometer, in which exercise intensity was progressively increased. The exercise intensity showed a ramp incremental to exhaustion. The starting power output was 20 W and an increase in power output of 0.5 W·s-1 was used. During the test, the following signals were measured: ECG by using the BioHarness 3.0 by Zephy; ventilation, oxygen and carbon dioxide concentration of the inhaled and exhaled air and a direct respiratory signal by using the metabolimeter. Other data were calculated and provided such as the HRs and the RFs. These latter ones were acquired and calculated using the turbine present within the metabolimeter, allowing a reliable estimation of RF during the exercise. In fact, the metabolimeter represents the gold standard in the respiratory signal and RF acquisition. For this reason, the RFs from the test have been used as reference values in order to evaluate the RF estimation from the EDR.

The duration of the tests changes slightly between subjects with an average of 14:43±1:1 minutes.

3.1.2 Pre-processing

Matlab was the working environment used in this study. The used version was the R2019b. The original sampling frequencies were 250 Hz and 50 Hz for the ECG and the respiratory signal, respectively. The signals were loaded into Matlab and resampled at a frequency of 200 Hz.

The following step was the pre-filtering. To remove high-frequency components, in both ECG and respiratory signals a low-pass filter (6rd order, bilinear Butterworth filter) was used with cut-off frequencies of 45 Hz and 1 Hz, respectively. In addition, the ECG signal was filtered with a high-pass filter (6rd order, bilinear Butterworth filter) with a cut-off frequency of 0.5 Hz, frequency usually used for diagnostic purposes.

Both ECG and respiratory signals were subdivided in consecutive windows with a duration of 30 s and subsequently analyzed using the proposed procedure.

3.1.3 Segmented-Beat Modulation Method for Electrocardiogram Derived Respiration

Ideally, the ECG can be thought of as a periodic signal obtained thanks to the repetition of many waveforms that represent a single beat. In reality, the ECG is a pseudo-periodic signal, since no beat contained in the ECG is equal to the others, in fact they could change in terms of morphology and duration. This physiological variability is due, in addition to control by the central nervous system, respiration, non-voluntary movements and non-physiological sources of noise [9].

To eliminate noise, the ECG is usually pre-filtered with linear techniques. These, however, do not eliminate the noise frequency components present within the ECG frequency band. Despite being corrupted by "surviving" noises from filtering, the ECG morphology is distinguishable and this is especially true for the R peak sequences, being the most prominent ECG waves [9].

Originally, the Segmented-Beat Modulation Method (SBMM) has been proposed as a filtering procedure capable, not only of obtaining a signal not corrupted by noise, but also of reconstructing each beat according to its original morphology and duration.

The SBMM works under the hypothesis of knowing the positions of the R peaks and the ECG is considered to be the repetition of N cardiac cycles (CC), which can differ in terms of duration and amplitude. In SBMM the beginning of the CC is identified in the P-Q segment (between the end of the P wave and the beginning of the Q wave), precisely $\Delta t = 40$ ms before the R peak. In addition, the SBMM is based on the observation that, in a first approximation, the QRS complex has a duration independent of HR, while the duration of all the other ECG waves varies with it. Specifically, the duration of the QRS complex is independent of the previous R-R interval, but the duration of the other waves is proportional to it. Under these considerations, each CC can be divided into two segments, the QRS and the TUP. The QRS segment is identified at $\pm \Delta t$ ms around the R peak, while the TUP segment is identified between Δt ms after the R peak and Δt ms before the next R peak. Each CC is characterized by its duration (Figure 23). However, the duration of all QRS segments is the same in all CCs (twice Δt), while the duration of TUP segments depends on CC [9].

According to the SBMM procedure, the sequence of R peaks containing the position of the R peaks within the noisy ECG is used to identify all the CCs and calculate the median of the RR interval (mRR). Before processing mCCs, all CCs are modulated in such a way that their duration is equal to mRR. Since the QRS segments are constant, the modulation concerns only the TUP segments and is obtained through elongations and linear compressions. Eventually, the modulated mCC provides a clean model of all the noisy ECG CC. Before chaining the N modulated mCCs to have a clean ECG at the exit of the SBMM procedure, the TUP segment of the mCC is demodulated (with compressions or elongations) to ensure that its duration is equal to the original duration of the TUP segment in the corresponding CC present in the noisy ECG. Then these CCs are reconstructed and optimization processes are used (i.e. to compensate for non-linear changes in HR) [9].

The SBMM was used both on simulated data, i.e. ideal traces produced using the MATLAB ECG simulator, and on ECG recordings of healthy subjects affected by various noise levels. In both cases, the SBMM has proven to be a useful tool for estimating ECG clean from noisy recordings and its robustness compared to other methods, such as the Standard Template Method (STM), has also been confirmed. Despite this, the noise due to electrode movement artifacts is the most difficult to filter. In normal cases where the amplitude of the QRS complex is higher than the noise (good signal/noise ratio), algorithms designed specifically to individuate the R peaks (such as Pan-Tompkins) can be applied. In cases where the R peaks are not directly derivable from the original noisy recording, the R peaks must be obtained indirectly, for example by using another ECG trace specifically intended for this purpose. Figure 25 shows the block diagram of the original SBMM [9].

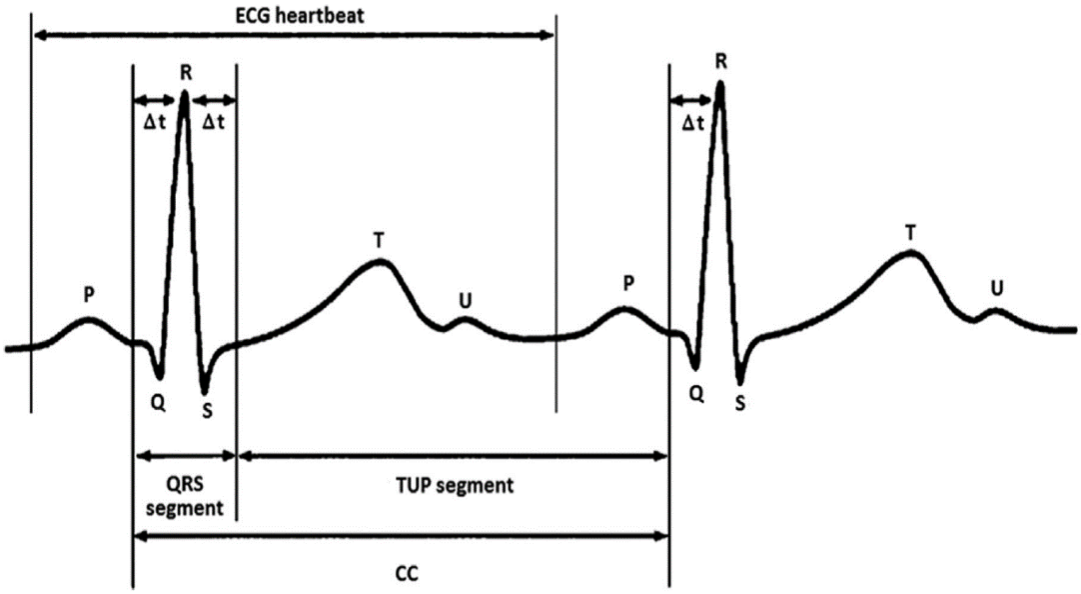

Figure 23. Typical ECG waveforms from which it is possible to identify the heartbeat that begins and ends at the beginning of the P wave and a specific CC, which begins and ends at the beginning of the Q wave, divided into the QRS and TUP segments [9].

The scheme of the used approach for the EDR extraction obtained from the mSBMM is shown in Figure 24 and three main steps were performed: pre-filtering, already discussed in the 'Pre-proccessing' section, mSBMM application and respiration signal derivation [36].

After the pre-filtering, the R-peaks were individuated by using algorithms designed for that purpose, such as Pan-Tompkins. Both the filtered ECG and the R peaks were used as inputs to the mSBMM.

The original SBMM includes an optimization process that makes each extracted beat as much as possible similar, in amplitude, to the original one. In this case, there would be an unnecessary adjustment of the ECG amplitude since the idea is to not filter the ECG modulation introduced by the respiration [36]. Figure 26 depicts the mSBMM, where the optimization processes on the demodulated CC are not present.

A clean ECG not affected by the respiration was provided as output from the mSBMM, differently from the input ECG modulated by the respiration. At this point, the EDR was derived by subtraction between the original modulated ECG and the clean ECG signals [36].

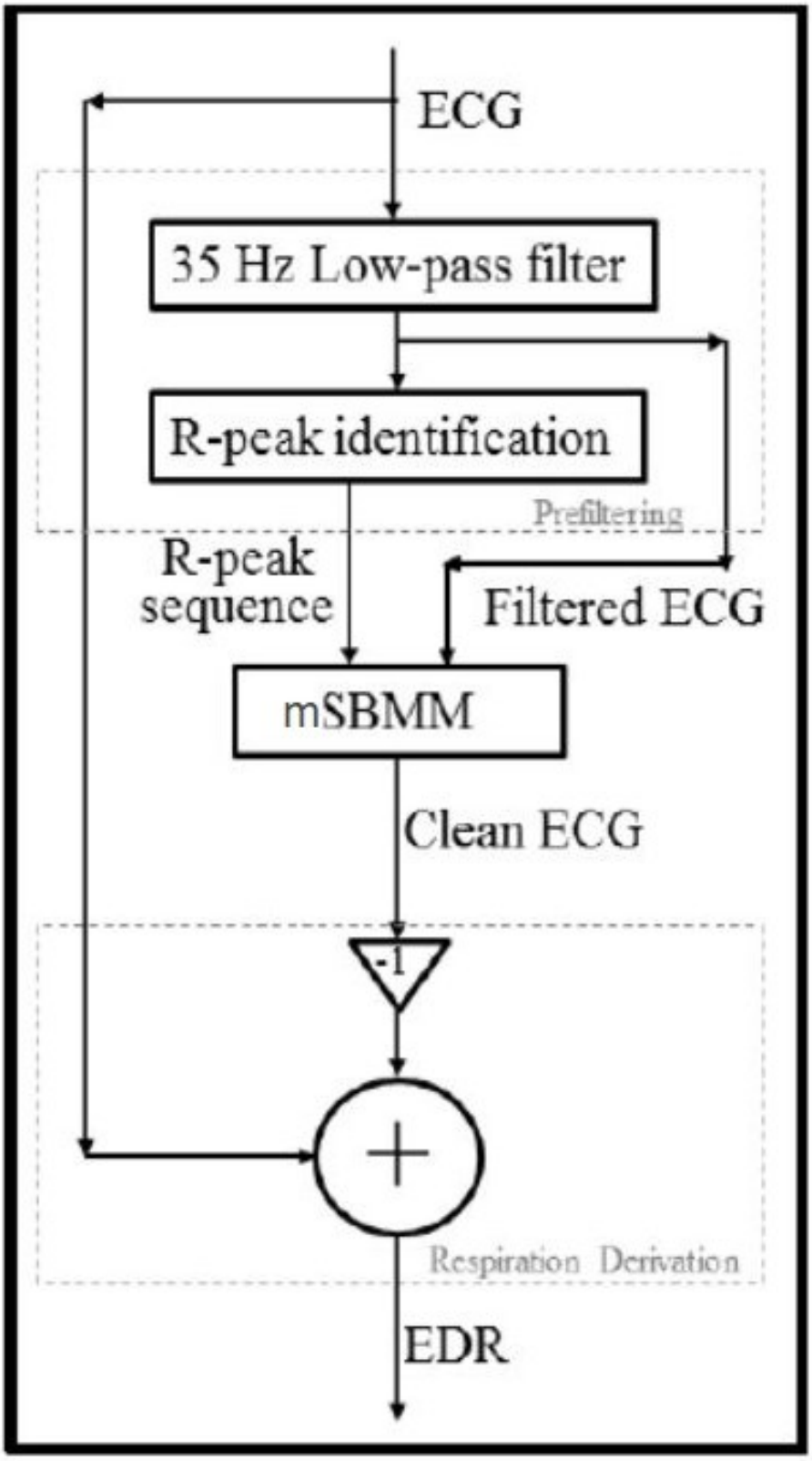

Figure 24. Extraction of the EDR through mSBMM [36]

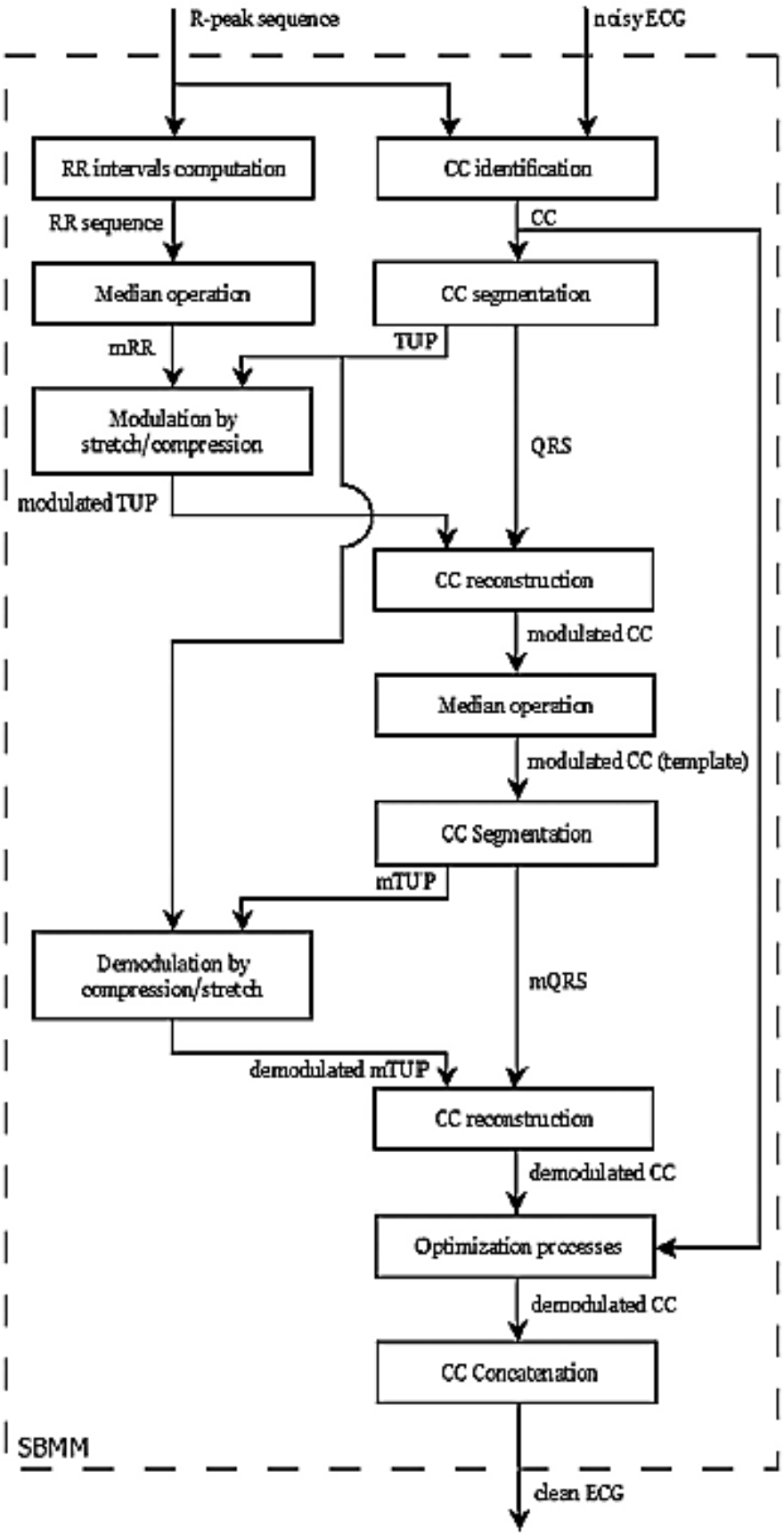

Figure 25. The original SBMM [7].

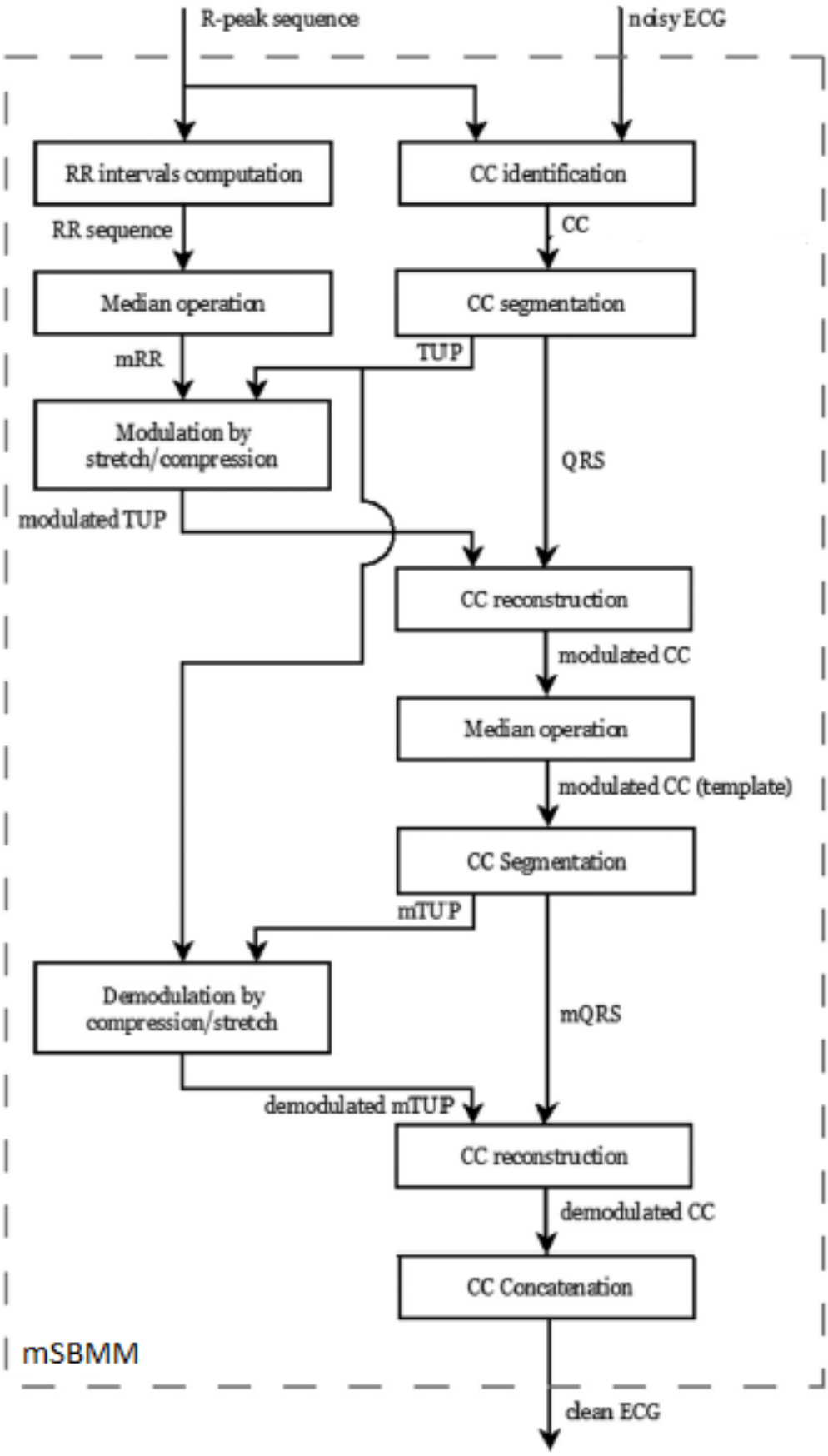

Figure 26. The mSBMM for EDR extraction [36].

3.1.3 Respiratory Frequency Model and the Respiratory Frequency Identification

The model was defined considering the HR and RF values collected from the nine subjects presented in the 'clinical data' section. This type of protocol allowed the collection of a large and significant range of HRs and RFs.

In order to avoid outliers and compromise the RF identification, a physiological range was considered. From a physiological point of view, during a physical activity the human body uses more oxygen and produces more carbon dioxide. To cope with this situation, the RF increases from about 15 cpm to 40-60 cpm [37]. For these reasons, all the values not included in the range between 15-65 cpm were excluded from the model definition because they were not physiological plausible.

Subsequently, the provided HR and RF values for each subject were loaded in the Curve Fitting App (or cftool) supplied by Matlab. This app is a flexible interface where it is possible to interactively fit curves and surfaces to data and view plots. The regression equation was calculated and the data was fitted by a double exponential curve expressed as:

$$\mathrm{y} = a * e^{b*x} + c * e^{d*x} \quad (5)$$

Then, the process to identify the RF by using the model involves several steps. Above all, in the considered subject the HR was calculated from the ECG. This value was used as input to the model determining a precise value of RF, called theoretical RF. A range of ±5 cpm was individuated starting from the theoretical RF. Then, the previously defined RF band was used to individuate the frequency at which the magnitude spectrum of the EDR had a maximum. Figure 27 summarizes the performed steps.

3.1.5 Statistics

Accuracy in RF estimation was assessed between the RFs from EDR, estimated using the proposed model, and the reference RFs comparing and evaluating the median (25^{th} and 75^{th} percentile) value, the correlation coefficients, both the absolute and relative errors and the p-values from the Wilcoxon signed-rank test. Statistical significance was set at 0.05.

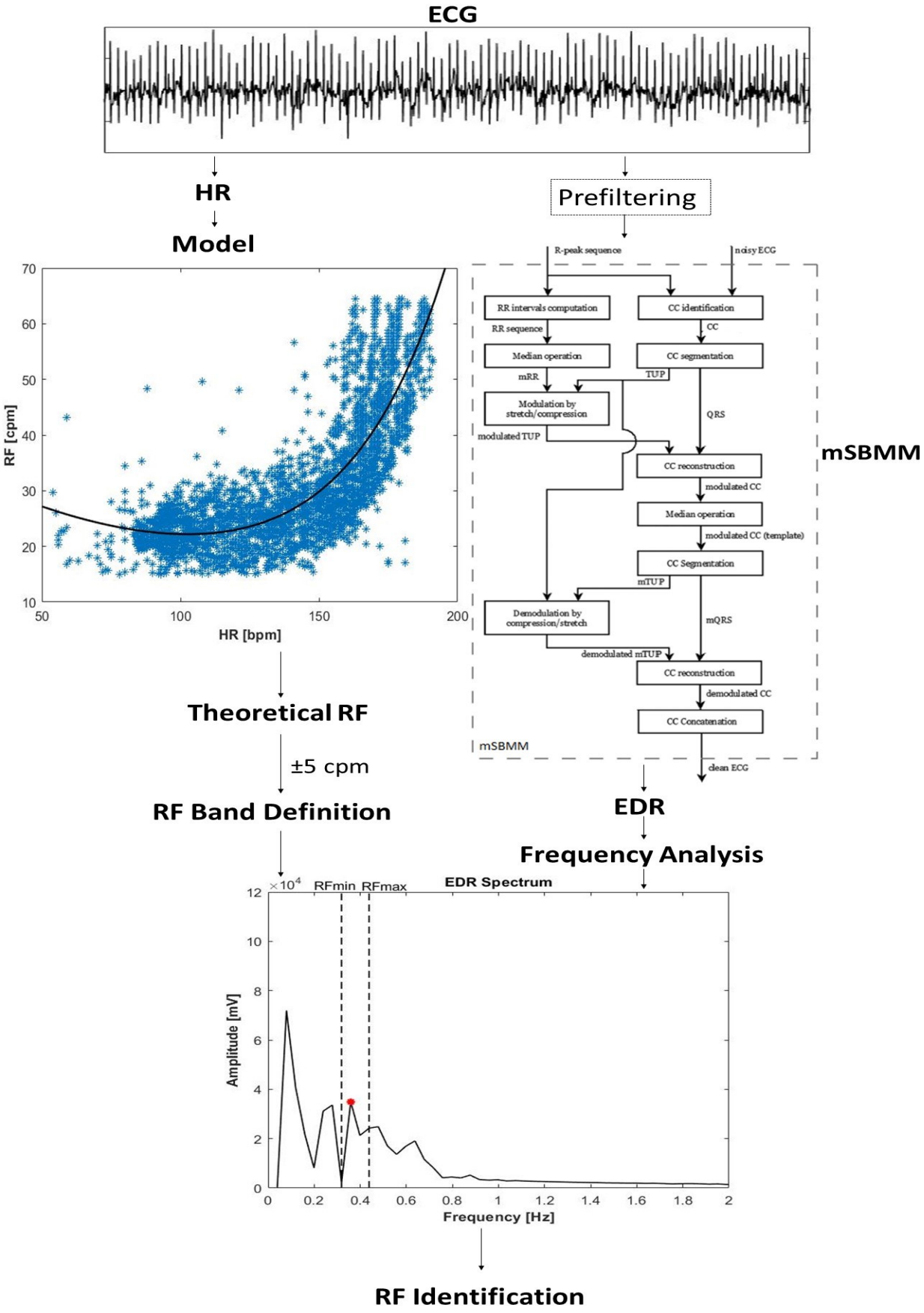

Figure 27. Flow chart summarizing the steps in order to calculate the RF from the EDR by using the model.

3.2 Results

HR and RF values were interpolated by using a double exponential. The coefficients of the exponential provided by the Curve Fitting App (or cftool) for the equation (5) are equal to:

- a=38.42;
- b=-0.007813;
- c=0.3065;
- d=0.02713.

Figure 28 shows the obtained model. ECG and respiratory signal were divided in windows with a duration of 30s, as shown in Figure 29. The respiratory signal and the corresponding EDR, obtained as output from the mSBMM, are compared in Figure 30. An example of the results obtained from the spectral analysis is reported in Figure 31. This window was a particular good case, in which the EDR spectrum had a clear dominant frequency as the respiratory signal one. In many other cases, this condition did not occur and the RF range, calculated from the model, was applied to EDR spectrum in order to improve the RF estimation (Figure 32, 33, 34). Median values for the comparison of RF values between EDR and RF distributions are reported in Table 3. In the same table, correlation coefficients, absolute and relative errors between the two distributions are reported.

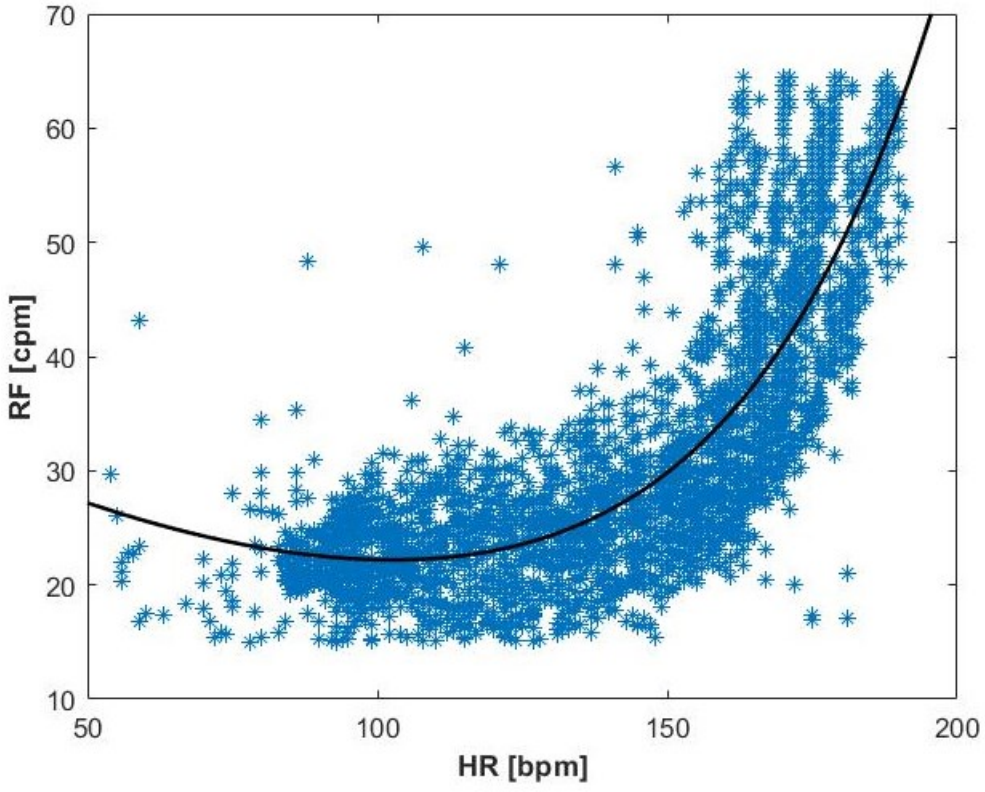

Figure 28. Model showing the relation between the HRs and RFs.

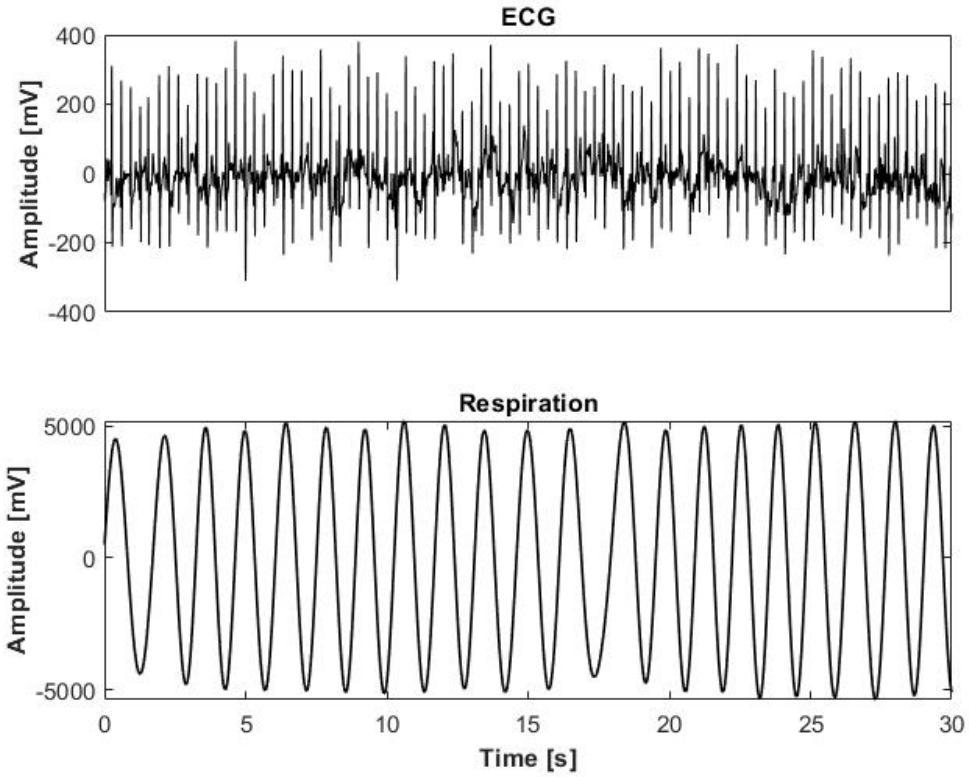

Figure 29. Example of a 30 s window of ECG and respiration signals.

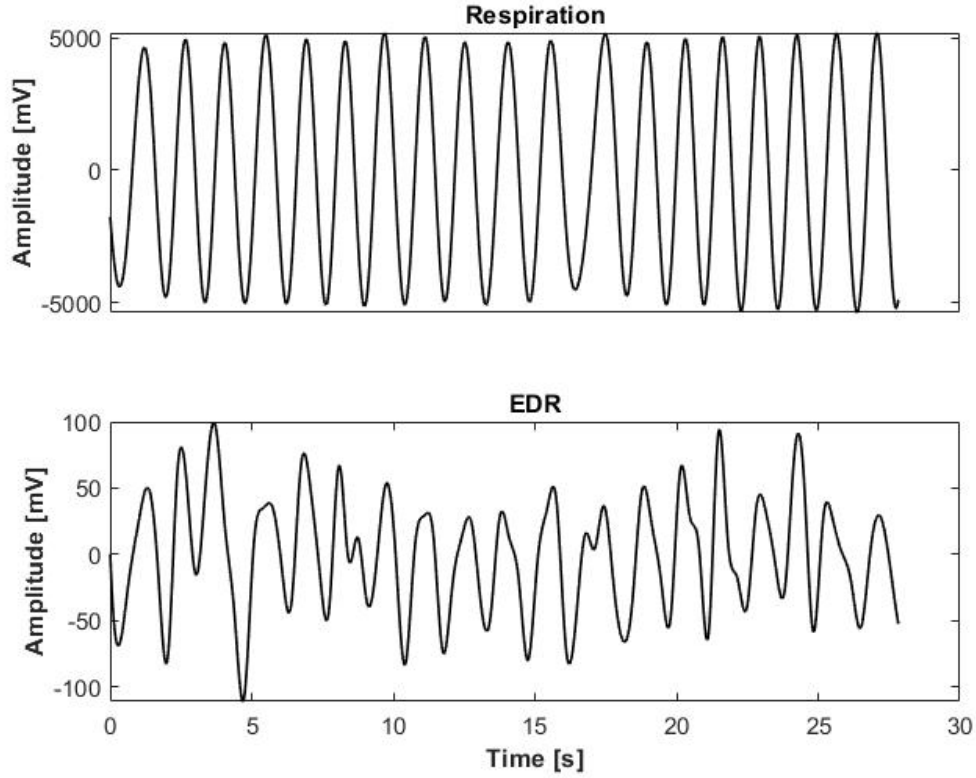

Figure 30. Example of respiration signal and EDR, obtained as output from mSBMM.

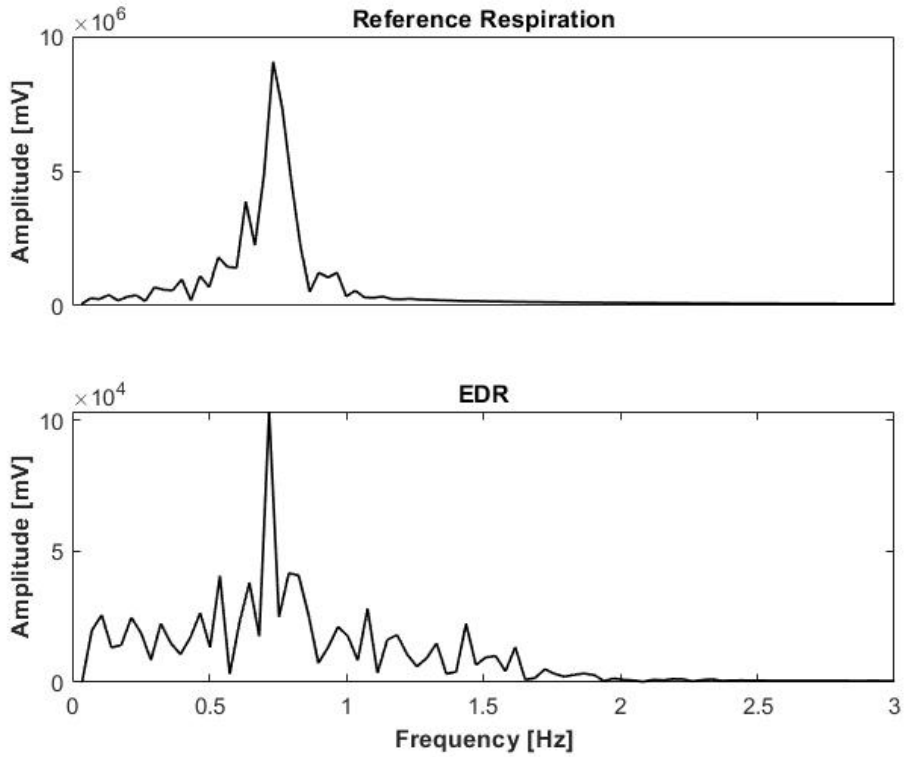

Figure 31. Spectra of the reference respiration signal and EDR.

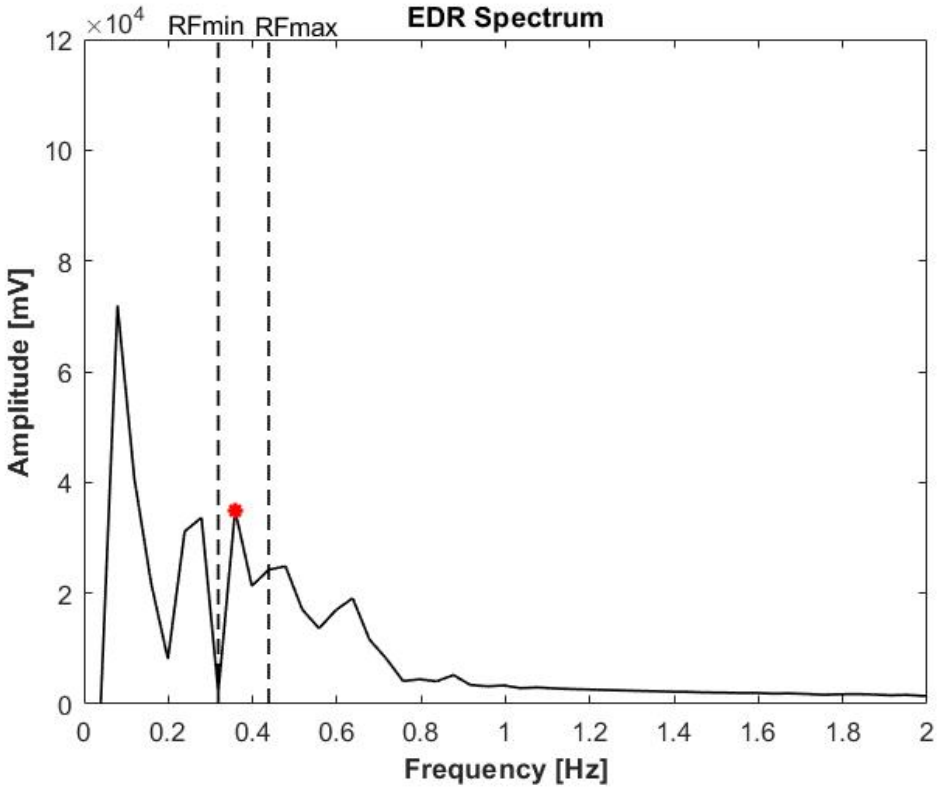

Figure 32. Example of the RF individuation as maximum of the frequency spectrum (red star) in the frequency range defined by the model.

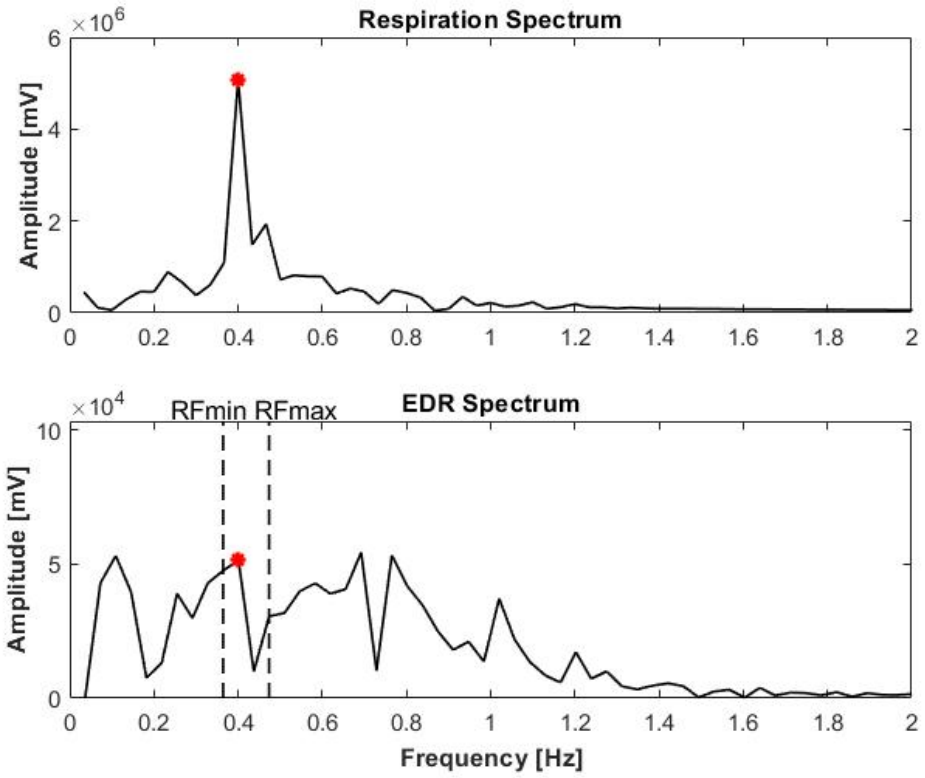

Figure 33. Example of the RF individuation in the frequency range defined by the model for the EDR. In this case, the model individuates that the RF is 0.4 Hz, as for the direct respiration signal.

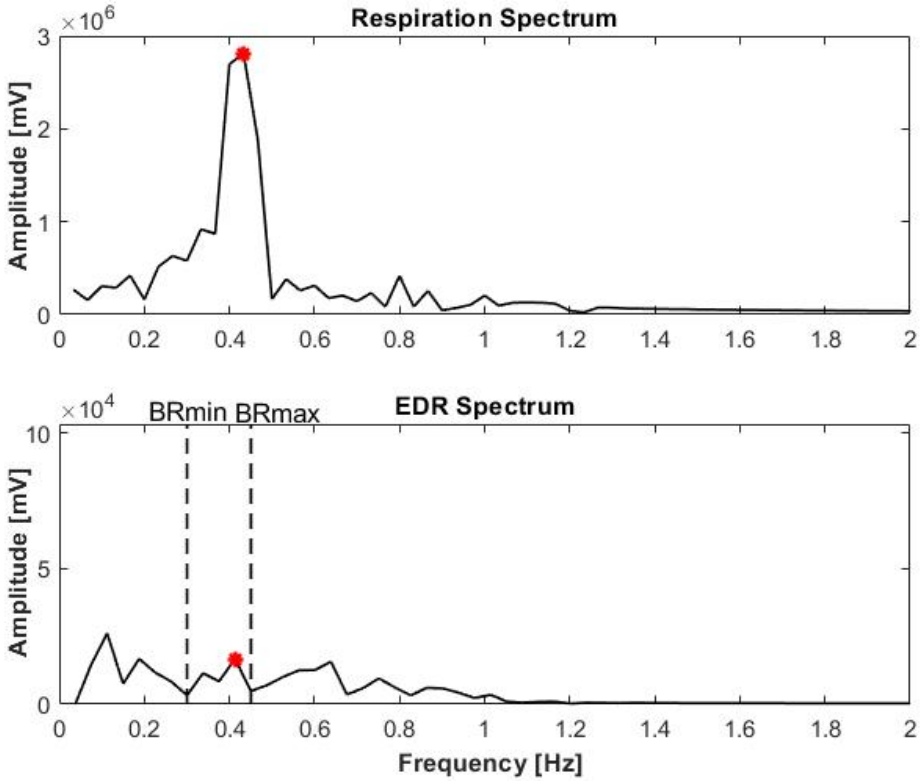

Figure 34. Example of the RF individuation in the frequency range defined by the model for the EDR. In this case, the model individuates that the RF is 0.4 Hz, as for the direct respiration signal.

Table 3. Values of EDR, RF and HR distribution reported for each subject from Roma Database. Correlation coefficients (R) and their p-values (P) to evaluate the significance level between RF/EDR distributions. Median absolute errors between RF/EDR distributions (ErrRF/EDRm). Median relative errors (ErrRel) between RF/EDR distributions expressed as percentage. In the last row (Tot) values are expressed as median value. sub: subjects; №: numbers; m: median; $_{25}$p: 25th percentile; $_{75}$p: 75th percentile; cpm: cycles per minute; bpm: beat per minute.

Sub	**Windows** (**№**)	**EDRm** (cpm) [$_{25}$p;$_{75}$p]	**RFm** (cpm) [$_{25}$p;$_{75}$p]	**HRm** (bpm) [$_{25}$p;$_{75}$p]	**Corr EDR/RF R(P)**	**ErrRF/EDRm** (cpm) [$_{25}$p;$_{75}$p]	**ErrRel RF/EDRm** [$_{25}$p;$_{75}$p] (%)
1	23	22.8 [20.1;24.5]	22 [20.2;26.2]	125 [102;138]	0.6 (2.5E-3)	-0.2 [-2.6;2.6]	-1 [-12.2;12.2]
2	27	26.2 [24.4;30.6]	23.9 [22.6;24.8]	129 [115;152]	0.8 (4.8E-6)	-2.2 [-5.7;0.5]	-12 [-25.6;2]
3	26	26.2 [22.1;28.5]	23.5 [20.4;30.2]	139 [123;156]	0.9 (1.3E-9)	-0.5 [-2.4;1.4]	-2 [-11.8;4.3]
4	26	30.4 [24.3;36.9]	26.5 [20.8;36.6]	154 [136;166]	0.8 (5.5E-6)	-3.1 [-5.8;3]	-13 [-24.3;12.4]
5	28	27.7 [23.9;29.7]	27.6 [26.8;34.3]	137 [120;149]	0.1 (0.6)	1.8 [-1.5;8.5]	7 [-5.6;30.9]
6	23	26.1 [22.4;29]	30.3 [25.5;32.7]	129 [115;147]	0.8 (1.3E-6)	6.1 [1.7;7.2]	15 [-5.6;22.9]
7	28	24.4 [20.6;34]	20.4 [18.2;29.2]	140 [125;165]	0.7 (6.3E-6)	-2.8 [-4.1;-1.9]	-13 [-18.7;-9.3]
8	28	29.7 [25.5;45.3]	29 [23;40.1]	153 [135;177]	0.8 (1.3E-8)	-1.4 [-3.4;0.9]	-6 [-13.8;2.6]
9	30	27.5 [25.1;30.3]	24.4 [22.8;30.5]	141 [128;150]	0.8 (1.6E-6)	-1.7 [-3.9;2.2]	-7 [-17.3;7.7]
Tot	239	26.2 [23.9;30.3]	24.4 [22.6;30.5]	139 [123;152]	0.8 (4.8E-6)	-1.4 [-3.4;2.2]	-6 [-13.8;7.7]

3.3 Discussion

Several are the algorithms proposed for the EDR extraction. Some of these are suitable during the sleep testing [38], other during more stressful testing [35]. There are algorithms that require more than one leads [7] or others to whom it is sufficient to use a single-lead [36]. Some leads seem to be more sensitive to the respiration due to their positioning, such as lead II and V4. However, in some cases, especially during sleep test, the choice of the lead is limited due to the electrode placement [38].

Usually, once that the position of the R peaks has been identified, most of the previous methods used to estimate the respiratory signal from the ECG use a straight line passing through the identified points and subsequently the segment is interpolated. Thus, the EDR is obtained.

In this study, a single- lead SBMM-based method and a model are proposed in order to estimate the EDR and identify in a reliable way the RF during physical exercise. One of the advantages in using SBMM is the possibility to choose the most suitable lead. Moreover, SBMM does not require extra sensors in achieving the purpose of the EDR extraction. In fact, with appropriate adjustments, the use of the SBMM allows to obtain the EDR considering the physiological variability between the clean ECG signal and the original shifted ECG signal, both obtained as output from the algorithm. The correct R peak sequence is essential for SBMM to work properly. However, R peak identification is almost always possible and not challenging. Therefore, at each peak R the difference between the two output signals is estimated, obtaining the EDR. After the extraction of the EDR through the SBMM, the frequency analysis of the EDR and the direct respiration was performed in order to individuate the RF. It is already known in literature that the frequency at which the spectrum had the higher amplitude corresponds to the RF [16]. Usually, especially for a subject at rest, this maximum is found in the range between 4 and 60 cpm (0.07 and 1 Hz, respectively). In presence of spectra with more than one peak, the frequency corresponding to the peak closest to 0.2 Hz is identified as the RF [35]. This occurs because 0.2 Hz is the frequency corresponding to the average number of respiratory acts per minute performed by an adult (12 cpm) [16].

However, in some cases, noises and interferences in the signal may comprise the individuation of this maximum and the relative RF identification. Similar situations can occur, for example, during exercise or wearing wearable sensors. For these reasons, the definition of a model and a RF frequency band in which individuate the maximum amplitude of the spectrum could be an important issues in order to increase the estimation accuracy and reliability.

The model was defined by fitting the HRs and RFs values collected by nine subjects applying a physiological range. Generally, it has been reported that during physical activity the RF increases from a resting value of 15 cpm up to about 40-60 cpm. This occurs because the human body has to cope the extra demand of oxygen and remove more carbon dioxide [40]. For this reason, in order to exclude possible outliers and increase the accuracy of the RF identification, in the present study all the RFs out of range 15-65 cpm were excluded.

As shown in Figure 27, the subject HR was used as input to the model. The model individuated as output a theoretical RF. The next step involved identifying a range of plausible frequencies in which the RF from the EDR had to lie within. This range was defined by considering ±5 cpm from the theoretical RF, individuating a maximum and minimum RF. As final step, the maximum of the EDR spectrum was individuate within the defined RF range. In order to assess the model performance in estimating the RF, the same subjects used for its definition were used for the SBMM application and EDR extractions.

A clear example of the usefulness of the model in RF estimation is shown in Figure 33. Indeed, the EDR spectrum exhibits several oscillations and its maximum amplitude is not clear. However, the application of the RF range in the spectrum allows the identification of a RF equal to 0.4 Hz, the same value found for the direct respiration spectrum where instead the maximum is clearly distinguishable.

From the table, some important results can be noticed. In the majority of the cases, the proposed procedure seems to slightly overestimate the RF value respect the reference RF (Table 3). The median RF value among the subjects from the EDR is 26.2 cpm against 24.2 cpm from the reference RF, leading to the mentioned slight overestimation (Table 3).

Table 3 reports the correlation coefficients and their significance levels between the RF/EDR distributions. A correlation coefficient is a numerical measure of some type of correlation, meaning a statistical relationship between two variables or distributions. A median correlation coefficient of 0.8 is obtained between the EDRs and the reference RFs. Except for a subject, all the correlation coefficients are greater than 0.6. It is an important result, because means that the RFs from the EDR can be considered the same as the reference RFs.

Absolute and relative errors in the estimation of RF from the EDR with respect the reference RF are reported in Table 3. The absolute errors were reported as signed differences between the RFs from reference RFs and the EDRs. The worst error occurred for the 6^{th} subject, where it was equal to -6.1 cpm. In the almost all the other subjects the errors are in an acceptable interval, ranges between 0.2 and 3 cpm. Overall, these findings are good and acceptable, considering that the subjects were performing a physical exercise and the resulting large range of the RFs, where an error of almost 2 cpm can be considered negligible. Among all subjects a final median error of -1.4 cpm is obtained in the RF estimation. In the same table, also the relative errors expressed as percentage calculated with respect the reference RFs were reported. As mentioned above, the worst case occurred for the 6^{th} subject with a median relative error of 15%. The majority of the subjects showed a relative error lower than the 10% and the median relative error among all subjects is equal to -6%.

The Wilcoxon signed-rank test is a non-parametric statistical hypothesis test used to compare two related samples, matched samples, or repeated measurements on a single sample to assess whether their population mean ranks differ (i.e. it is a paired difference test). A Wilcoxon signed-rank test can be used to determine whether two dependent samples were selected from populations having the same distribution. Results confirm that the RF from EDR and the RF distributions on average are not statistically significant (p-value=0.1). It is possible to confirm that what has been extracted with the EDR is the equivalent of that obtained from the reference RF.

Chapter 4: Conclusions

The results showed that the RFs extracted by the EDR tend to slightly overestimate the reference RFs, with 26.2 cpm and 24.4 cpm respectively. Expect for a subject, correlation coefficients between EDR and reference RFs reported the strength of the relationship between the two distributions.

Absolute errors of RF estimation, calculated as signed differences, were on average very low. In fact, the error between RFs obtained from the EDR and the reference RFs is on average -1.4 cpm, which is an acceptable value during a physical exercise. In the majority of the cases, the relative error expressed as percentage from the reference RF was lower than the 10%.

The outcomes from the Wilcoxon signed-rank test show that these distributions are not statistically significant on average, confirming that what it was extracted from the EDR was comparable with what obtained from both the reference RFs.

From results, it is possible to confirm how the mSBMM is a powerful tool in the extraction of the EDR also during physical exercise. The defined model, although its simplicity, allows a more reliable and accurate RF identification from the EDR in a situation other than that of rest. However, in this model only a parameter, the HR, was considered in order to individuate the RF. In practice, several different parameters and complex processes are involved in the RF identification and its variation. This would require a deeper study of the physiological mechanisms involved in order to define a more robust model.

A further investigation could concern the choice of the most appropriate range for the RF identification from the theoretical RF provided by the model. Moreover, future studies will evaluate this method to a larger population, including both healthy subjects and those with respiratory problems. The proposed procedure may be tested on longer ECG tracings. One of main advantages of the mSBMM is that it does not require extra sensors or the acquisition of other additional signals to provide the EDR. For this reason, another interesting aspect may be to use the proposed procedure in the long-term, possibly real-time, monitoring through wearable sensors or smartphone applications.

Bibliography

[1] Elliott, Malcolm. (2016). Why is Respiratory Rate the Neglected Vital Sign? A Narrative Review. International Archives of Nursing and Health Care. 2. 10.23937/2469-5823/1510050.

[2] Mazzanti, B., Lamberti, C., & de Bie, J. (2003). Validation of an ECG-derived respiration monitoring method. *Computers in Cardiology, 2003*, 613–616. https://doi.org/10.1109/cic.2003.1291230.

[3] Nicolò, A., Massaroni, C., & Passfield, L. (2017). Respiratory Frequency during Exercise: The Neglected Physiological Measure. *Frontiers in physiology*, *8*, 922. https://doi.org/10.3389/fphys.2017.00922.

[4] Charlton, P. H., Bonnici, T., Tarassenko, L., Alastruey, J., Clifton, D. A., Beale, R., & Watkinson, P. J. (2017). Extraction of respiratory signals from the electrocardiogram and photoplethysmogram: technical and physiological determinants. *Physiological Measurement*, *38*(5), 669–690. https://doi.org/10.1088/1361-6579/aa670e.

[5] Scholkmann, F., & Wolf, U. (2019). The Pulse-Respiration Quotient: A Powerful but Untapped Parameter for Modern Studies About Human Physiology and Pathophysiology. *Frontiers in physiology*, *10*, 371. https://doi.org/10.3389/fphys.2019.00371.

[6] American Institute Of Physics. (2007, February 1). Heartbeat And Breathing Cycles. *ScienceDaily*. Retrieved July 10, 2020 from www.sciencedaily.com/releases/2007/01/070130122437.htm.

[7] Moody, G., Roger, M., Zoccola, A., & Mantero, S. (1985). Derivation of Respiratory Signals from Multilead ECGs. *Computers in Cardiology, 12*.

[8] Caggiano, D., & Reisman, S. (1996). Respiration derived from the electrocardiogram: a quantitative comparison of three different methods. *Proceedings of the IEEE 22nd Annual Northeast Bioengineering Conference*, 103–104. https://doi.org/10.1109/nebc.1996.503238

[9] Agostinelli, A., Sbrollini, A., Giuliani, C., Fioretti, S., Nardo, F. D., & Burattini, L. (2016). Segmented beat modulation method for electrocardiogram estimation from noisy recordings. *Medical engineering & physics*, *38*(6), 560–568.

[10] Ambrosi, G., Castano, P., & Donato, R.F. (2006). *Anatomia dell'uomo*, *seconda edizione*. Edi. Ermes.

[11] Branca, F. P., Cannella, M., Galo, J., M., Rubegni, S., & Silvestri, S. (2000). *Fondamenti di Ingegneria Clinica - Volume 1 (Italian Edition)* (2000th ed.). Springer.

[12] Sörnmo, L., & Laguna, P. (2005). *Bioelectrical Signal Processing in Cardiac and Neurological Applications (Biomedical Engineering)* (1st ed.). Academic Press.

[13] Becker D. E. (2006). Fundamentals of electrocardiography interpretation. *Anesthesia progress*, *53*(2), 53–64. https://doi.org/10.2344/0003-3006(2006)53[53:FOEI]2.0.CO;2.

[14] *All About Heart Rate (Pulse). (2017). Www.Heart.Org. https://www.heart.org/en/health-topics/high-blood-pressure/the-facts-about-high-blood-pressure/all-about-heart-rate-pulse.*

[15] Benchetrit G. (2000). Breathing pattern in humans: diversity and individuality. *Respiration physiology*, *122*(2-3), 123–129. https://doi.org/10.1016/s0034-5687(00)00154-7.

[16] Mazeika G.G., Swanson R. (2007). *Respiratory Inductance Plethysmography an Introduction*. Pro-Tech Services, Inc., 5–8.

[17] Charlton, P. H., Birrenkott, D. A., Bonnici, T., Pimentel, M., Johnson, A., Alastruey, J., Tarassenko, L., Watkinson, P. J., Beale, R., & Clifton, D. A. (2018). Breathing Rate Estimation From the Electrocardiogram and Photoplethysmogram: A Review. *IEEE reviews in biomedical engineering*, *11*, 2–20. https://doi.org/10.1109/RBME.2017.2763681.

[18] Karlen, Walter & Raman, Srinivas & Ansermino, Mark & Dumont, Guy. (2013). Multiparameter Respiratory Rate Estimation From the Photoplethysmogram. IEEE transactions on bio-medical engineering. 60. 1946-1953. 10.1109/TBME.2013.2246160.

[19] Charlton, P. H., Bonnici, T., Tarassenko, L., Clifton, D. A., Beale, R., & Watkinson, P. J. (2016). An assessment of algorithms to estimate respiratory rate from the electrocardiogram and photoplethysmogram. *Physiological Measurement*, *37*(4), 610–626. https://doi.org/10.1088/0967-3334/37/4/610.

[20] Ruangsuwana, R., Velikic, G., & Bocko, M. (2010). Methods to extract respiration information from ECG signals. *2010 IEEE International Conference on Acoustics, Speech and Signal Processing*, 570–573. https://doi.org/10.1109/icassp.2010.5495584.

[21] Widjaja, D., Varon, C., Dorado, A., Suykens, J. A. K., & Van Huffel, S. (2012). Application of Kernel Principal Component Analysis for Single-Lead-ECG-Derived Respiration. *IEEE Transactions on Biomedical Engineering*, *59*(4), 1169–1176. https://doi.org/10.1109/tbme.2012.2186448.

[22] Engelse, W.A.H., Zeelenberg, C. (1979). A single scan algorithm for QRS detection and feature extraction. *IEEE Computers in Cardiology*, 37-42.

[23] Sakai, Motoki & Zhu, Xin & Yoshida, Yuki & Wei, Daming. (2013). Development of Lead System for ECG-Derived Respiration Aimed at Detection of Obstructive Sleep Apnea Syndrome. *International Conference on Signal-Image Technology and Internet-Based Systems,* 971-975. 10.1109/SITIS.2013.157.

[24] Alikhani, I., Noponen, K., Hautala, A., Ammann, R., & Seppänen, T. (2017). Spectral Data Fusion for Robust ECG-derived Respiration with Experiments in Different Physical Activity Levels. *Proceedings of the 10th International Joint Conference on Biomedical Engineering Systems and Technologies*, 88–95. https://doi.org/10.5220/0006144100880095.

[25] K.Rajkumar, K. (2013). Respiration Rate Diagnosis using Single Lead ECG in Real Time. *Global Journal Of Medical Research, 13,* 7–11.

[26] Sobron, A. & Romero, I. & Lopetegi, Txema. (2010). Evaluation of methods for estimation of respiratory frequency from the ECG. *Computing in Cardiology, 37*, 513 - 516.

[27] Lázaro, J., Alcaine, A., Romero, D., Gil, E., Laguna, P., Pueyo, E., & Bailón, R. (2014). Electrocardiogram derived respiratory rate from QRS slopes and R-wave angle. *Annals of biomedical engineering*, *42*(10), 2072–2083. https://doi.org/10.1007/s10439-014-1073-x.

[28] Noriega, M., Maranon, E. J., Romero, D., Orini, M., & Almeida, R. (2016). Respiratory rate estimation from multilead directions, based on ECG delineation. *2016 38th Annual International Conference of the IEEE Engineering in Medicine and Biology Society (EMBC)*, 3813–3816. https://doi.org/10.1109/embc.2016.7591559.

[29] Sierra-Alonso, E.F., Sepúlveda-Cano, L.M., Bailon-Luesma, R., Laguna, P., Pablo & Castellanos-Dominguez, G. (2013). Estimating respiratory frequency from HRV during treadmill exercise testing. *Computing in Cardiology, 40*,121-124.

[30] Berset, T., Romero, I., Young, A., & Penders, J. (2012). Robust heart rhythm calculation and respiration rate estimation in ambulatory ECG monitoring. *Proceedings of 2012 IEEE-EMBS International Conference on Biomedical and Health Informatics*, 293–296. https://doi.org/10.1109/bhi.2012.6211599.

[31] Helfenbein, E., Firoozabadi, R., Chien, S., Carlson, E., & Babaeizadeh, S. (2014). Development of three methods for extracting respiration from the surface ECG: a review. *Journal of electrocardiology*, *47*(6), 819–825. https://doi.org/10.1016/j.jelectrocard.2014.07.020.

[32] Espiritu Santo, A., & Carbajal, C. (2010). Respiration rate extraction from ECG signal via discrete wavelet transform. *2010 2nd Circuits and Systems for Medical and Environmental Applications Workshop (CASME)*, 1–4. https://doi.org/10.1109/casme.2010.5706679.

[33] Schäfer, A., & Kratky, K. W. (2008). Estimation of breathing rate from respiratory sinus arrhythmia: comparison of various methods. *Annals of biomedical engineering*, *36*(3), 476–485. https://doi.org/10.1007/s10439-007-9428-1.

[34] Yi-Hsin, C., Hau-Tieng, W., & Shu-Shya, H. (2011). ECG-derived respiration and instantaneous frequency based on the synchrosqueezing transform: application to patients with atrial fibrillation. [online] Available: https://arxiv.org/vc/arxiv/papers/1105/1105.1571v1.pdf.

[35] Bailon, R., Pahlm, O., Sornmo, L., & Laguna, P. (2004). Robust electrocardiogram derived respiration from stress test recordings: validation with respiration recordings. *Computers in Cardiology, 2004*, 293–296. https://doi.org/10.1109/cic.2004.1442930.

[36] Pambianco, B., Sbrollini, A., Marcantoni, I., Morettini, M., Fioretti, S., & Burattini, L. (2018). Electrocardiogram Derived Respiratory Signal through the Segmented-Beat Modulation Method. *Conference proceedings : ... Annual International Conference of the IEEE Engineering in Medicine and Biology Society. IEEE Engineering in Medicine and Biology Society. Annual Conference*, *2018*, 5681–5684. https://doi.org/10.1109/EMBC.2018.8513493.

[37]Your lungs and exercise. (2016). *Breathe*, *12*(1), 97–100. https://doi.org/10.1183/20734735.elf121.

[38] Park, S.-B., Noh, Y.-S., Park, S.-J., & Yoon, H.-R. (2008). An improved algorithm for respiration signal extraction from electrocardiogram measured by conductive textile electrodes using instantaneous frequency estimation. *Medical & Biological Engineering & Computing*, *46*(2), 147–158. https://doi.org/10.1007/s11517-007-0302-y.